

# Effects of Turbulent Environment and Random Noise on Self-Organized Critical Behavior: Universality vs Nonuniversality

N. V. Antonov,<sup>\*</sup> N. M. Gulitskiy,<sup>†</sup> P. I. Kakin,<sup>‡</sup> and V. D. Serov  
*Department of Physics, Saint Petersburg State University,  
 7/9 Universitetskaya nab., Saint Petersburg 199034, Russia*

Self-organized criticality in the Hwa-Kardar model of “running sandpile” [*Phys. Rev. A* **45**, 7002 (1992)] with a turbulent motion of the environment taken into account is studied with the field theoretic renormalization group (RG). The turbulent flow is modeled by the synthetic  $d$ -dimensional anisotropic velocity ensemble introduced by Avellaneda and Majda [*Commun. Math. Phys.* **131**: 381 (1990)] with finite correlation time. The Hwa-Kardar model with time-independent (spatially quenched) random noise is considered alongside the original model with the white noise. The aim of the present paper is to explore fixed points of RG equations which determine the possible types of universality classes (regimes of critical behavior of the system) and critical dimensions of the measurable quantities. Our calculations demonstrate that influence of the type of the random noise is extremely large: in contrast to the case of the white noise where the system possess three fixed points, the case of the spatially quenched noise involves four fixed points with overlapping stability regions. This means that in the latter case the critical behavior of the system depends not only on the global parameters of the system which is the usual case, but also on the initial values of the charges (coupling constants) of the system. These initial conditions determine the specific fixed point which will be reached by RG flow. Since now the critical properties of the system are not defined strictly by its parameters the situation may be interpreted as universality violation. Such systems are not forbidden but they are very rare. It is especially interesting that the same model without turbulent motion of the environment does not predict this nonuniversal behavior and demonstrates the “usual” one with prescribed universality classes instead [*J. Stat. Phys.* **178**, 392 (2020)].

## I. INTRODUCTION

Since its introduction, the concept of self-organized criticality (SOC) [1] – [7] has been a focus of constant attention and scrutiny [8] – [11]. In a stark contrast to equilibrium systems that display critical scaling (long-time and large-distance asymptotic behavior with universal exponents) when a tuning parameter (e.g., the temperature) approaches a critical value [12] – [14], the systems with SOC arrive at the critical state due to their intrinsic dynamics. This “self-tuning” is observed in various open nonequilibrium systems with dissipative transport including biological systems [15, 16], their subclass neural systems [17] – [22], online social network systems [23] – [28], and various others. As advanced data analysis and sophisticated computational methods become more available, researchers from various fields increasingly turn to the concept of SOC. For example, in [29] SOC was used to explain connection between crop losses and extreme climate events while in [30] crisis behavior in autism spectrum disorders was analyzed as a self-tuned critical state.

SOC is usually described by discrete models, with discrete space and time evolution. For example, in [23] the model of a disordered system of interacting spins was used to determine the primary mechanism for self-tuning in a social system (social network for human collaborative knowledge creation). Nevertheless, universal scaling properties of SOC can be studied using simplified continuous models for smoothed (coarse-grained) fields. Indeed, this approach proved to be fruitful for investigation of critical behavior of various discrete systems. For example, it was found that the discrete Ising and Heisenberg models of equilibrium critical behavior belong to the universality class of the continuous  $O(n)$ -symmetric  $\varphi^4$  model; see [12] – [14]. A nonequilibrium example is provided by growth phenomena and fluctuating surfaces [31], where numerous discrete models are believed to belong to the universality class of the continuous Kardar-Parisi-Zhang model [32, 33]; for a recent discussion of reaction-diffusion models see [34]. The conserved directed-percolation related to the Manna universality class of SOC is also often studied by continuous models, see recent papers [35, 36].

In papers [37, 38], Hwa and Kardar proposed an anisotropic stochastic differential equation as a continuous model for a system with SOC. The equation describes evolution of a sandpile surface that undergoes changes as new sand enters the system and triggers avalanches (“running” sandpile). The surface has a flat average slope that determines the preferred direction for sand transport.

---

<sup>\*</sup> n.antonov@spbu.ru

<sup>†</sup> n.gulitskiy@spbu.ru

<sup>‡</sup> p.kakin@spbu.ru

Let us describe the model. The stochastic equation for the scalar field  $h(x) = h(t, \mathbf{x})$  that denotes a deviation of the sand profile height from its average value is taken in the form

$$\partial_t h = \nu_{\perp 0} \partial_{\perp}^2 h + \nu_{\parallel 0} \partial_{\parallel}^2 h - \partial_{\parallel} h^2 / 2 + f. \quad (1.1)$$

A unit constant vector  $\mathbf{n}$  defines the preferred direction, so any vector  $\mathbf{x}$  decomposes as  $\mathbf{x} = \mathbf{x}_{\perp} + \mathbf{n} x_{\parallel}$  where  $(\mathbf{x}_{\perp} \cdot \mathbf{n}) = 0$ . This leads to the appearance of the two spatial derivatives: a  $(d - 1)$ -dimensional gradient  $\partial_{\perp}$  and one-dimensional gradient  $\partial_{\parallel}$ . The first one  $\partial_{\perp} = \partial / \partial x_i$  with  $i = 1, \dots, (d - 1)$  is the derivative in the subspace orthogonal to  $\mathbf{n}$ , the second one is defined as  $\partial_{\parallel} = (\mathbf{n} \cdot \partial)$ . Symbol  $d$  denotes the spatial dimension,  $\partial_t = \partial / \partial t$ ,  $\partial_{\perp}^2 = (\partial_{\perp} \cdot \partial_{\perp})$ ,  $\nu_{\parallel 0}$  and  $\nu_{\perp 0}$  are two diffusivity coefficients, and  $f(x)$  is a random noise. Traditionally, the nonlinear term  $\partial_{\parallel} h^2 / 2$  would have a coupling constant as a factor. Here the fields and the parameters were rescaled to make this factor equal to unity (the coupling constant, thus, appears in the amplitude of the correlator for the random noise  $f$ ).

Different types of the random noise correspond to different physical systems and, as we will see, lead to completely different critical properties. A white noise  $f_w(x)$ , i.e., a Gaussian random noise with a zero mean and pair correlation function of a form

$$\langle f_w(x) f_w(x') \rangle = C_0 \delta(t - t') \delta^{(d)}(\mathbf{x} - \mathbf{x}'), \quad C_0 > 0, \quad (1.2)$$

was used in [37, 38]. A generalization of the Hwa-Kardar model with this noise and the coupling constant that was also considered to be a random field was proposed and studied in [39]. A model similar to (1.1) – (1.2) with the nonlinearity  $\propto \partial_{\parallel}^2 h^3$  was introduced in [40, 41] and discussed in relation to erosion of landscapes<sup>1</sup>.

In addition to (1.2), the authors of [40, 41] studied the case of the time-independent (spatially quenched) noise with correlation function

$$\langle f_s(x) f_s(x') \rangle = D_0 \delta^{(d)}(\mathbf{x} - \mathbf{x}'), \quad D_0 > 0. \quad (1.3)$$

Notably, it turned out that the model [40, 41] predicts nontrivial behavior only for the case of spatially quenched noise (1.3) [44]. Moreover, this behavior is nonuniversal [44].

Originally, the noise (1.3) was proposed in [47] to reflect the existence of nonerodible (“quenched”) regions of landscape in the problem of erosion. This choice was motivated by the experimental results that had revealed that heterogeneity of the soil is likely the main factor leading to scaling in erosion [48]. The spatially quenched noise (1.3) and its more general form that depends on the field  $h$  (see Eq. (1.1)) were also studied in [49] – [52]. In particular, the connection of this noise to nonuniversality in relation to directed percolation was discussed in [53] – [55].

In general, the random noise is an essential part of a model. It incorporates various random processes that affect the system while satisfying underlying symmetries of the problem, e.g., the Galilean symmetry. Thus, the choice of the noise is one of the key steps in the model construction. Then, it is natural to expect that the change of the noise would greatly affect the model.

However, the exact effect of the type of noise on the scaling behavior is difficult to predict. For example, analysis of the Hwa-Kardar model (1.1) with the spatially quenched noise (1.3) did not reveal any universality classes with unexpected features [45, 46]. It was shown in [56, 57] that the stochastic Navier-Stokes equation with temporally correlated noise reveals the same scaling properties as if the noise was white in-time. On the other hand, it was recently reported that temporally correlated noise in the KPZ model causes anomalous scaling behavior [58]. So this effect seems to be an important avenue to explore.

The critical behavior of the system can be greatly affected by the turbulent flows present in the environment; see, e.g., [59] – [69]. The advection by the velocity field  $\mathbf{v}(x)$  can be introduced by the “minimal” replacement in the Eq. (1.1):

$$\partial_t \rightarrow \nabla_t = \partial_t + (\mathbf{v} \cdot \partial). \quad (1.4)$$

Here  $\nabla_t$  is the Galilean covariant (Lagrangian) derivative.

The Hwa-Kardar model (1.1) with turbulent flow was studied in [70]. In that work the noise was chosen in the form (1.2) while a  $d$ -dimensional generalization of the velocity ensemble introduced earlier by Avellaneda and Majda [71, 72] was adopted as velocity statistics. This ensemble can be considered as an anisotropic version of the Kazatsev-Kraichnan “rapid-change” ensemble; the latter attracted enormous attention on the turn of the Millennium within the turbulent community because of the deep insight it offered into the origins of intermittency and anomalous scaling in fluid turbulence; see [73] and references therein.

Since the model (1.1) has an intrinsic strong anisotropy (preferred direction for sand transport) it is natural to use an anisotropic ensemble for velocity statistics too. In the real physical system, the velocity field  $\mathbf{v}(x)$  should obey stochastic Navier-Stokes equation. But to consider it instead of synthetic ensemble with prescribed statistics seems to be a very complicated task that we presently postpone for the future. In this paper we try instead to move forward by using a more realistic modification of the mentioned above Avellaneda and Majda ensemble which incorporates finite correlation time.

<sup>1</sup> It should be noted that such a modification leads to drastic changes in the RG analysis: the model [40, 41] appears renormalizable only in its extended version that involves infinitely many coupling constants; see [42] – [46] for discussion.

Let us describe it in detail. Following [71, 72] and subsequent works we take the velocity field in the form

$$\mathbf{v} = \mathbf{n} v(t, \mathbf{x}_\perp), \quad (1.5)$$

where  $v(t, \mathbf{x}_\perp)$  is a scalar amplitude. Thus defined, the velocity field is incompressible: the scalar function  $v(t, \mathbf{x}_\perp)$  does not depend on  $x_\parallel$ , therefore,  $(\partial \cdot \mathbf{v}) = \partial_\parallel v(t, \mathbf{x}_\perp) = 0$ .

The statistical velocity ensemble employed in this paper is a  $d$ -dimensional generalization of the ensemble with finite correlation time introduced in [74]; see also [75] – [82]. It was studied later (also in the short-correlated version) in [67], [83] – [85] in connection with the effects of turbulent motion on the dynamic critical behavior and in [86] – [90] in connection with the problem of anomalous scaling of passively advected scalar and vector fields. It can also be viewed as an anisotropic modification of the ensemble studied in [91] – [94] in connection with the anomalous scaling in fluid turbulence and in [66] – [69] in connection with the effects of turbulent motion on the critical behavior.

The amplitude velocity coefficient  $v(t, \mathbf{x}_\perp)$  has a Gaussian distribution with a zero mean and prescribed pair correlation function

$$\langle v(t, \mathbf{x}_\perp) v(t', \mathbf{x}'_\perp) \rangle = \int \frac{d\omega}{2\pi} \int_{k>m} \frac{d\mathbf{k}}{(2\pi)^d} e^{i\mathbf{k}(\mathbf{x}-\mathbf{x}')-i\omega(t-t')} B_v(\omega, \mathbf{k}), \quad (1.6)$$

where

$$B_v(\omega, \mathbf{k}) = 2\pi\delta(k_\parallel) B_0 \frac{k_\perp^{5-d-(\xi+\eta)}}{\omega^2 + (\alpha_0 v_{\perp 0} k_\perp^{2-\eta})^2}. \quad (1.7)$$

Here  $k_\perp = |\mathbf{k}_\perp|$  while infrared (IR) regularization in the form of the sharp cutoff  $k > m$  (which is equal to  $k_\perp > m$ ) is chosen for the convenience. Other parameters beside  $m$  in Eqs. (1.6) – (1.7) include constant positive amplitude factor  $B_0$ , a new parameter  $\alpha_0$  needed for dimensional consistency, and two arbitrary exponents  $\xi$  and  $\eta$ . The role of the exponent  $\xi$  could be glimpsed from the asymptotic law of the one-dimensional velocity spectrum:

$$\mathcal{E}(k_\perp) \sim k_\perp^{d-2} B_0 \int \frac{d\omega}{2\pi} \frac{k_\perp^{5-d-(\xi+\eta)}}{\omega^2 + (\alpha_0 v_{\perp 0} k_\perp^{2-\eta})^2} = \frac{B_0}{2\alpha_0 v_{\perp 0}} k_\perp^{1-\xi}. \quad (1.8)$$

The exponent  $\eta$ , on the other hand, appears in the dispersion law

$$\omega(k_\perp) \sim k_\perp^{2-\eta}. \quad (1.9)$$

The notation  $z = 2 - \eta$  is sometimes used in the literature instead; see, e.g., [72].

The specific choice of the velocity correlation function (1.6), (1.7) is justified by connection with the stochastic Navier-Stokes equation [86]. The substitution (1.5) “kills” the nonlinearity in the Navier-Stokes equation:  $(\mathbf{v} \cdot \partial) v_i = n_i v(t, \mathbf{x}_\perp) \partial_\parallel v(t, \mathbf{x}_\perp) = 0$ . The equation becomes linear and, thus, determines a Gaussian distribution known as the Ornstein-Uhlenbeck process [95, 96]. An appropriate power-like choice of the effective viscosity coefficient and the correlation function of the stirring force lead to the correlation function (1.6), (1.7).

In contrast to the rapid-change model where correlation function depends on time  $t$  as  $\delta(t - t')$ , our choice (1.6) – (1.7) has power dependence on the frequency  $\omega$ . What is important is that depending on  $\alpha_0$  it allows for two special cases interesting on their own. The limit  $\alpha_0 \rightarrow 0$  at fixed  $B_0/\alpha_0$  corresponds to the case of “frozen” or “quenched” velocity field that does not depend on time. The correlator (1.6) then turns into  $B_v \sim \delta(\omega) k^{3-d-\xi}$ . The limit  $\alpha_0 \rightarrow \infty$  at fixed  $B_0/\alpha_0^2$  returns us to the vanishing correlation time (“rapid-change” case) where  $\langle v(t, \mathbf{x}_\perp) v(t', \mathbf{x}'_\perp) \rangle \sim \delta(t - t')/k_\perp^{d-1+\tilde{\xi}}$  and  $\tilde{\xi} = \xi - \eta$ . The exponent  $0 < \tilde{\xi} < 2$  is, in a sense, a Hölder’s exponent that indicates “roughness” of the velocity field. A smooth velocity is associated with the “Batchelor limit”  $\tilde{\xi} \rightarrow 2$  while the most realistic velocity corresponds to the Kolmogorov value  $\tilde{\xi} = 4/3$  [73]. Thus, the Kolmogorov values of the exponents  $\xi$  and  $\eta$  are  $8/3$  and  $4/3$ , respectively.

In the present paper, we study two models of SOC with field theoretic RG approach. The first model consists of the stochastic equation (1.1) with the white in-time noise (1.2) subjected to the turbulent stirring (1.4) – (1.7). The second model differs from the first one only in the choice of the random noise in the equation (1.1), i.e., the spatially quenched noise (1.3) is used instead of the white noise (1.2). As we will see, obtained results are completely different. Both of the models can be reformulated as quantum field theories so their possible large-scale, long-distance asymptotic regimes are associated with IR attractive fixed points of the RG equations.

There are two different ways to organise this paper. On the one hand, we analyze two specific models and obtain specific results so it is possible to present these two models separately, i.e., in series. On the other hand, we want to stress how the type of the noise affects the results; for this reason it is more convenient to present two models in parallel. We chose the latter way.

What is the most interesting is that there are no significant differences between the two models even in the obtained  $\beta$  functions: for both models they are very similar to each other, and it is impossible to predict the huge difference in following analysis at first glance. In our opinion, this is the most interesting point, and, thus, we chose the organisation of the paper that highlighted it.

We hope that we will not cause too much inconvenience to the reader with the use of repeating symbols for different cases: since the starting equation (1.1) and some others are the same for both models, this is unavoidable.

The paper is organized as follows. In Sec. II the field theoretic formulations of the models are presented and Feynman diagrammatic technique is introduced. In Sec. III renormalization of the models (divergent Green functions, renormalized actions, and constants  $Z$  needed for multiplicative renormalization) is discussed. Sec. IV is devoted to RG equation, RG functions, and IR attractive fixed points connected to them. In Sec. V critical scaling and critical dimensions in different scaling regimes are discussed. Sec. VI is reserved for conclusion. The main result is that the set of the fixed points for the model with the spatially quenched noise is much more complicated than the same set for the model with the white noise.

Appendixes A and B contain some details of the calculations. Since it is a technical point, we do not discuss any details of the calculations in the main text; herewith, it may be useful or interesting at some point to see them.

## II. FIELD THEORETIC FORMULATION OF THE MODELS

From now on, every section is organised as follows: we start with the model that involves the white noise (1.2) which we refer to in text as Model 1. Then we consider the model with the spatially quenched noise (1.3); this model is referred to as Model 2.

According to the general theorem, any stochastic differential equation with one time derivative and  $t$ -local functional that depends on the fields and their spatial derivatives of arbitrary types and orders is equivalent to some field theory with action  $\mathcal{S}(\Phi)$ ; see, e.g., [97] – [99] and monographs [13, 14]. This equivalence means that statistical averages of random quantities in initial stochastic problem coincide with functional averages with weight  $\exp \mathcal{S}(\Phi)$ . This idea appears to be very fruitful and allows one to apply well-known techniques of quantum field theory like Feynman diagrammatic technique, renormalization and RG equation, operator product expansion, etc., to problems of statistical physics.

### A. Model 1: The model with the white noise

The action  $\mathcal{S}(\Phi)$  mentioned above for stochastic problem (1.1), (1.2), (1.4), (1.6) involves the fields  $\Phi = \{h', h, v\}$  and reads

$$\mathcal{S}(\Phi) = \frac{1}{2} h' D_0 h' + h' \left\{ -\partial_t h - v \partial_{\parallel} h + v_{\perp 0} \partial_{\perp}^2 h + v_{\parallel 0} \partial_{\parallel}^2 h - \partial_{\parallel} h^2 / 2 \right\} + \mathcal{S}_v. \quad (2.1)$$

Here  $h'$  is auxiliary (response) field and all integrations over  $x = \{t, \mathbf{x}\}$  and summations over vector indices are implied; for instance,

$$\frac{1}{2} h' D_0 h' = \frac{1}{2} \int dt d\mathbf{x} h'(t, \mathbf{x}) h'(t, \mathbf{x}). \quad (2.2)$$

The term  $\mathcal{S}_v$  describes the Gaussian averaging over the velocity field  $v$ :

$$\mathcal{S}_v = \frac{1}{2} \int dt d\mathbf{x}_{\perp} d\mathbf{x}'_{\perp} v(t, \mathbf{x}_{\perp}) \widetilde{B}_v^{-1}(\mathbf{x}_{\perp} - \mathbf{x}'_{\perp}) v(t, \mathbf{x}'_{\perp}), \quad (2.3)$$

where  $\widetilde{B}_v^{-1}$  is the kernel of the linear operation  $B_v^{-1}$  which is the inverse operation for the  $B_v$  in (1.7).

Feynman diagrammatic technique for the theory (2.1) involves four bare propagators. The velocity propagator  $\langle vv \rangle_0$  is defined in (1.6). Other three propagators that contain the height field  $h$  and response field  $h'$  in the frequency-momentum representation read

$$\langle hh \rangle_0 = \frac{D_0}{\omega^2 + \epsilon^2(k)}, \quad \langle hh' \rangle_0 = \langle h' h \rangle_0^* = \frac{1}{-i\omega + \epsilon(k)}, \quad \langle h' h' \rangle_0 = 0, \quad (2.4)$$

where we denote  $\epsilon(k) = v_{\parallel 0} k_{\parallel}^2 + v_{\perp 0} k_{\perp}^2$ .

The nonlinear terms  $-h' \partial_{\parallel} h^2 / 2$  and  $-h'(v \partial_{\parallel}) h$  define the vertices  $V_{h'hh}$  and  $V_{h'vh}$ . It is convenient to define the corresponding coupling constants  $g_0$  and  $w_0$  by the relations

$$D_0 = g_0 v_{\parallel 0}^{3/2} v_{\perp 0}^{(d_L-1)/2}, \quad B_0 = w_0 v_{\parallel 0} v_{\perp 0}^2. \quad (2.5)$$

where  $d_L$  is logarithmic dimension of the model. Then, canonical dimension analysis (see Sec. III for details) gives  $g_0 \sim \ell^{-\epsilon}$  and  $w_0 \sim \ell^{-\xi-\eta}$ , where  $\ell$  sets the smallest length scale in the problem (ultraviolet cutoff) and  $\epsilon = 4 - d$ . The parameter  $\alpha_0 \sim \ell^{-\eta}$  should be considered alongside the coupling constants. Indeed, although it is not an expansion parameter in the perturbation theory, the RG function will depend on its renormalized analog.

### B. Model 2: the model with the spatially quenched noise

Now let us turn to Model 2. As the previous one, it can be reformulated as a field theory of the set of three fields  $\Phi = \{h', h, v\}$ . The action functional has the same form as Eq. (2.1) with the only difference: the first term now reads

$$\frac{1}{2} h' D_0 h' = \frac{1}{2} \int dt dt' \int dx h'(t', x) D_0 h'(t, x) \quad (2.6)$$

with the double integration over the time variables.

As Model 1, Model 2 also involves four bare propagators. The propagator  $\langle vv \rangle_0$  is still defined in (1.6); another three propagators in the frequency-momentum representation read

$$\langle hh \rangle_0 = \frac{2\pi\delta(\omega) D_0}{\epsilon^2(k)}, \quad \langle hh' \rangle_0 = \langle h'h \rangle_0^* = \frac{1}{-i\omega + \epsilon(k)}, \quad \langle h'h' \rangle_0 = 0, \quad (2.7)$$

where  $\epsilon(k)$  is defined by linear part of Hwa-Kardar equation and, therefore, is the same as for Model 1; see Eq. (2.4).

As before, the theory involves two vertices related to the interaction terms and three coupling constants:  $g_0$  and  $w_0$  defined by (2.5) and  $\alpha_0$ . From canonical dimension analysis (see Sec. III) it follows that  $g_0 \sim \ell^{-\tilde{\epsilon}}$ ,  $w_0 \sim \ell^{-\xi-\eta}$  and  $\alpha_0 \sim \ell^{-\eta}$  with  $\tilde{\epsilon} = 6-d$ .

### III. RENORMALIZATION OF THE MODELS

Ultraviolet (UV) divergences are determined through canonical dimensions analysis (“power counting”), see, e.g., [12] – [14]. Let us briefly detail the process. Firstly, one needs to find canonical dimensions of the fields and parameters of the theory. The strongly anisotropic dynamic theories like Model 1 and Model 2 have three independent scales: the time scale  $T$  and two length scales (in the corresponding subspaces)  $L_\perp$  and  $L_\parallel$ . Thus, a quantity  $F$  is described by three canonical dimensions:

$$[F] \sim [T]^{-d_F^\omega} [L_\perp]^{-d_F^\perp} [L_\parallel]^{-d_F^\parallel}.$$

The total canonical dimension  $d_F$  is a sum of the doubled frequency dimension  $d_F^\omega$  and the momentum dimensions  $d_F^\perp$  and  $d_F^\parallel$ :  $d_F = d_F^\perp + d_F^\parallel + 2 d_F^\omega$ . The free theory relation  $\partial_t \propto \partial_\perp^2 \propto \partial_\parallel^2$  explains the factor 2.

As each term of the action (2.1) is completely dimensionless ( $\sim [T]^0 [L_\perp]^0 [L_\parallel]^0$ ), the canonical dimensions can be easily calculated; the normalization conditions  $d_{k_\perp}^\perp = -d_{x_\perp}^\perp = 1$ ,  $d_{k_\perp}^\parallel = -d_{x_\perp}^\parallel = 0$ ,  $d_{k_\perp}^\omega = d_{k_\parallel}^\omega = 0$ ,  $d_\omega^\omega = -d_t^\omega = 1$  are assumed.

#### A. Model 1: the model with the white noise

The canonical dimensions for Model 1 are presented in Table I. The parameter  $\mu$  is the renormalization mass, i.e., the reference momentum scale defined by its canonical dimensions [14].

From Table I it follows that the model is logarithmic (all the coupling constants are dimensionless, or, in other words, all the interactions are marginal in the sense of Wilson) at  $\varepsilon = \xi = \eta = 0$ , where  $\varepsilon = 4 - d$ . Thus, these three exponents will serve as the expansion parameters in the RG theory.

Once canonical dimensions are found, the UV divergences can be analyzed. The UV divergence index of an arbitrary 1-irreducible Green function  $\Gamma = \langle \Phi \cdots \Phi \rangle_{1-ir}$  is given by the expression

$$\delta_\Gamma = d + 2 - N_{h'} d_{h'} - N_h d_h - N_v d_v |_{\varepsilon=\xi=\eta=0}, \quad (3.1)$$

where  $N_h$ ,  $N_{h'}$ ,  $N_v$  are the numbers of the corresponding fields in the function  $\Gamma$ .

TABLE I. Canonical dimensions of the fields and parameters in Model 1;  $\varepsilon = 4 - d$ .

$F$	$h'$	$h$	$D_0$	$\nu_{\parallel 0}$	$\nu_{\perp 0}$	$v$	$B_0$	$\alpha_0$	$g_0$	$w_0$	$\mu, m$
$d_F^\omega$	-1	1	3	1	1	1	3	0	0	0	0
$d_F^\parallel$	2	-1	-3	-2	0	-1	-2	0	0	0	0
$d_F^\perp$	$d-1$	0	$1-d$	0	-2	0	$\xi + \eta - 4$	$\eta$	$\varepsilon$	$\xi + \eta$	1
$d_F$	$d-1$	1	$4-d$	0	0	1	$\xi + \eta$	$\eta$	$\varepsilon$	$\xi + \eta$	1

If  $\delta_\Gamma$  is a nonnegative integer, then the function  $\Gamma$  may contain superficial UV divergences. Table I and expression (3.1) gives

$$\delta_\Gamma = 6 - 3N_{h'} - N_h - N_v. \quad (3.2)$$

There are additional considerations that should be taken into account when analyzing UV divergences. Firstly, since both vertices  $V_{h'hh}$  and  $V_{h'vh}$  allow to move derivative  $\partial_\parallel$  onto the field  $h'$  the real index of divergence reads

$$\delta'_\Gamma = \delta_\Gamma - N_{h'}. \quad (3.3)$$

Moreover, all 1-irreducible Green functions without response field  $h'$  involve closed circuits of retarded propagators  $\langle h'h \rangle_0$  and, thus, vanish [14]. So  $N_{h'} \geq 1$ .

The Galilean symmetry usually forbids some of the counterterms allowed by power counting and, therefore, reduces the number of counterterms. However, the correlation function (1.6) does not contain the Dirac function  $\delta(t - t')$  necessary for Galilean symmetry. This lack of symmetry may result in some “interesting physical pathologies” [100]. In the present case, though, due to the strong anisotropy of the theory (2.1) and incompressibility of the velocity, the action (2.1) is invariant under the following Galilean transformations

$$h(t, \mathbf{x}) \rightarrow h(t, \mathbf{x} + \mathbf{u}t), \quad h'(t, \mathbf{x}) \rightarrow h'(t, \mathbf{x} + \mathbf{u}t), \quad \mathbf{v}(t, \mathbf{x}) \rightarrow \mathbf{v}(t, \mathbf{x} + \mathbf{u}t) - \mathbf{u}, \quad (3.4)$$

where  $\mathbf{u} = n\mathbf{u}$ , which can be verified by the direct substitution. Expression (3.4) means that the scalar velocity changes as  $v(t, \mathbf{x}_\perp) \rightarrow v(t, \mathbf{x}_\perp) - u$  and  $\mathbf{x}_\perp$  remains unchanged in all of the fields in (3.4). This symmetry can be viewed as a residue of the full-scale Galilean symmetry that survived the substitution (1.5) made in the Navier-Stokes equation; see Sec. 9 in [86].

In our case this observation forbids counterterms for 1-irreducible functions with the field  $v$ , namely  $\langle h'v \rangle_{1-ir}$  with  $\delta_\Gamma = 2$ ,  $\langle h'hv \rangle_{1-ir}$  with  $\delta_\Gamma = 1$ , and  $\langle h'vv \rangle_{1-ir}$  with  $\delta_\Gamma = 1$ . Moreover, there are two types of graphs for function  $\langle h'hh \rangle_{1-ir}$  with  $\delta_\Gamma = 1$ : the one with propagator  $\langle vv \rangle$  inside the core (integrand) and the one without. The former is trivially equal to zero while the core of the graphs of the latter fully coincides with similar cores for the function  $\langle h'hv \rangle_{1-ir}$ . This means that the Galilean symmetry, in fact, forbids the possible counterterm for function  $\langle h'hh \rangle_{1-ir}$  too.

Taking all of the above into account, we can ascertain that only one counterterm has to be considered which is  $h'\partial_\parallel^2 h$  that appears from the 1-irreducible function  $\langle h'h \rangle_{1-ir}$  with  $\delta_\Gamma = 2$ . This means that Model 1 is renormalizable and renormalized action reads

$$\mathcal{S}_R(h, h', v) = \frac{1}{2} h' D h' + h' \left\{ -\partial_t h - v \partial_\parallel h + v_\perp \partial_\perp^2 h + Z_{v_\parallel} v_\parallel \partial_\parallel^2 h - \partial_\parallel h^2 / 2 \right\} + \mathcal{S}_v. \quad (3.5)$$

This renormalization can be reproduced by multiplicative renormalization of the parameters

$$g_0 = \mu^\varepsilon g Z_g, \quad w_0 = \mu^{\xi+\eta} w Z_w, \quad \alpha_0 = \alpha \mu^\eta, \quad \nu_{\parallel 0} = \nu_\parallel Z_{\nu_\parallel}, \quad \nu_{\perp 0} = \nu_\perp. \quad (3.6)$$

Here  $g$ ,  $w$ , etc., are renormalized counterparts of the bare parameters  $g_0$ ,  $w_0$ , etc.;  $\mu$  is renormalization mass, an additional parameter of the renormalized theory (see, e.g., [13, 14]). Due to the fact that there is only one counterterm, the fields  $h$ ,  $h'$  and  $v$  are not renormalized and following relations hold true:

$$Z_g = Z_{\nu_\parallel}^{-3/2}, \quad Z_w = Z_{\nu_\parallel}^{-1}.$$

The renormalization constant  $Z_{\nu_\parallel}$  can be calculated in the double series in  $g$  and  $w$ .

In the minimal subtraction (MS) scheme all the renormalization constants have the forms “ $Z = 1 +$  only poles in  $\varepsilon$ ,  $\xi$  and their combinations.” The leading-order (one-loop) calculation gives

$$Z_{\nu_\parallel} = 1 - \frac{1}{2\alpha(1+\alpha)} \frac{w}{\xi} - \frac{3}{16} \frac{g}{\varepsilon} \quad (3.7)$$

with the corrections of higher orders in  $g$  and  $w$ . Here and below we redefined the coupling constant  $g \rightarrow g S_d / (2\pi)^d$  where  $S_d = 2\pi^d / \Gamma(d/2)$  is the area of the unit sphere in the  $d$ -dimensional space; the same redefinition is also true for the second coupling constant  $w$ . Details of the calculations can be found in Appendix A.

## B. Model 2: the model with the spatially quenched noise

Now let us turn again to Model 2. Canonical dimensions for Model 2 are presented in Table II. The only difference between the two sets of canonical dimensions is the dimension of the parameter  $D_0$  which leads to a different dimension of the coupling constant  $g_0$ . This in turn leads to the shift of the logarithmic dimension of the model: now all of the couplings are dimensionless at  $\tilde{\varepsilon} = \xi = \eta = 0$  where  $\tilde{\varepsilon} = 6 - d$ .

The UV divergence index of an arbitrary 1-irreducible Green function  $\Gamma$  is given by Eq. (3.1) and reads

$$\delta_\Gamma = 8 - 5N_{h'} - N_h - N_v. \quad (3.8)$$

The spatially quenched noise (1.3) destroys Galilean symmetry (3.4) which is true for Model 1. This fact can be checked directly: the term (2.6) is not invariant under the transformations (3.4). Thus, in contrast to Model 1, we have to deal with all five types of divergent functions:  $\langle h'h \rangle_{1-ir}$ ,  $\langle h'v \rangle_{1-ir}$ ,  $\langle h'hw \rangle_{1-ir}$ ,  $\langle h'hh \rangle_{1-ir}$ , and  $\langle h'vv \rangle_{1-ir}$ .

Moreover, since propagator  $\langle hh \rangle_0$  in Eq. (2.7) is proportional to  $\delta(\omega)$ , Model 2 has an additional feature that leads to a reduction of counterterms: when a diagram involves  $n \geq 2$  inner lines  $\langle hh \rangle_0$ , it with necessity has  $(n-1)$  delta functions of external frequencies  $\delta(\Omega_i)$  as factors. Each factor contributes  $d_{\delta(\Omega_i)} = -2$  to the divergence index while being unrelated to the momenta divergence. Thus, the real index of divergence has an additional term  $2(n-1)$  and reads

$$\delta''_\Gamma = \delta_\Gamma - N_{h'} + 2(n-1). \quad (3.9)$$

The possible ‘‘dangerous’’ function of such type is  $\langle h'h' \rangle_{1-ir}$ . It has formal index of divergence  $\delta_\Gamma = -2$  but the one-loop approximation contains the graph with two lines  $\langle hh \rangle_0$ . This allows for a possibility that integral over momenta has a logarithmic divergence. However, the situation is safe due to the two vertices  $V_{h'hh}$  which are responsible for the term  $-N_{h'}$  in Eq. (3.9). Thus, the real index of divergence for this function  $\delta''_\Gamma = -2$  and we have no problems with it.

One more nontrivial observation for this model is worth mentioning. Usually when we state that a Green function is divergent we actually mean that there are divergences of the integrals over momenta, i.e., divergences of the Feynman graphs itself. But integrals over momenta are just a core of the Green functions: they should be contracted with external projectors, propagators or fields. If transverse vector fields are involved, such a contraction may lead to an unexpected vanishing of the result.

Consider the function  $\langle h'v \rangle_0$  whose index of divergence is  $\delta''_\Gamma = 1$ , so, according to the naive dimensional analysis, we should account for it in the renormalization procedure. However, owing to the vertex factor  $V_{h'hh}$ , each graph for this function is proportional to an external momenta  $p_\parallel$ . This feature along with the property  $\partial_\parallel v(t, \mathbf{x}_\perp) = 0$  [see Eq. (1.5)] leads to the fact that  $\langle h'v \rangle_0 = 0$  after contraction of the core of the graph with the ‘‘external’’ fields  $h'$  and  $v$ .

The same observation also holds for the function  $\langle h'vv \rangle_0$ : each graph contains two external momenta and the Green function itself involves two vector fields  $v$ . Thus, this function also vanishes, along with the corresponding counterterm.

The similar observation is no longer true for the function  $\langle h'hw \rangle_0$ : there is still two external momenta but the Green function itself involves only one vector field  $v$ . This means that some nontrivial divergent part survives the contraction.

The functions that contain four or more fields have negative real index of divergence  $\delta''_\Gamma$  and, therefore, are not needed for renormalization procedure from general requirements<sup>2</sup>.

Taking all of the above into account, we can ascertain that three counterterms has to be considered, which are  $h' \partial_\parallel^2 h$ ,  $h'v \partial_\parallel h$ , and  $h' \partial_\parallel h^2$  that appear from the 1-irreducible functions  $\langle h'h \rangle_{1-ir}$ ,  $\langle h'hw \rangle_{1-ir}$ , and  $\langle h'hh \rangle_{1-ir}$  correspondingly. Thus, Model 2 is multiplicatively renormalizable and renormalized action reads

$$\mathcal{S}(h, h', v) = \frac{1}{2} h' D h' + h' \{-\partial_t h - Z_v v \partial_\parallel h + v_\perp \partial_\perp^2 h + Z_{v_\parallel} v_\parallel \partial_\parallel^2 h - Z_h \partial_\parallel h^2 / 2\} + \mathcal{S}_v. \quad (3.10)$$

This procedure can be reproduced by multiplicative renormalization of the fields  $h \rightarrow h Z_h$ ,  $h' \rightarrow h' Z_{h'}$ ,  $v \rightarrow v Z_v$  and parameters

$$g_0 = \mu^{\tilde{\varepsilon}} g Z_g, \quad w_0 = \mu^{\xi+\eta} w Z_w, \quad \alpha_0 = \alpha \mu^\eta, \quad v_{\parallel 0} = v_\parallel Z_{v_\parallel}, \quad (3.11)$$

where  $g$ ,  $w$ , etc. are renormalized analogs of bare parameters and  $\mu$  is renormalization mass. The viscosity  $v_{\perp 0}$  remains the same:  $v_{\perp 0} = v_\perp$ . The relations

$$Z_{h'} = Z_h^{-1}, \quad Z_g = Z_h^2 Z_{v_\parallel}^{-3/2}, \quad Z_w = Z_v^2 Z_{v_\parallel}^{-1} \quad (3.12)$$

TABLE II. Canonical dimensions of the fields and parameters in Model 2;  $\tilde{\varepsilon} = 6 - d$ .

$F$	$h'$	$h$	$D_0$	$v_{\parallel 0}$	$v_{\perp 0}$	$v$	$B_0$	$\alpha$	$g_0$	$w_0$	$\mu, m$
$d_F^\omega$	-1	1	4	1	1	1	3	0	0	0	0
$d_F^\parallel$	2	-1	-3	-2	0	-1	-2	0	0	0	0
$d_F^\perp$	$d-1$	0	$1-d$	0	-2	0	$\xi + \eta - 4$	$\eta$	$\tilde{\varepsilon}$	$\xi + \eta$	1
$d_F$	$d-1$	1	$6-d$	0	0	1	$\xi + \eta$	$\eta$	$\tilde{\varepsilon}$	$\xi + \eta$	1

<sup>2</sup> We want to note that while this analysis is very convenient as it allows to reduce the number of the Green functions to consider from the very beginning, it is, in fact, not obligatory. If we do not perform it now, we will have to calculate graphs for more Green functions but some of them will be ‘‘occasionally’’ equal to zero.

result from the absence of renormalization of the other terms in (3.10).

Three independent constants  $Z_{\nu_{\parallel}}$ ,  $Z_v$ , and  $Z_h$  can be calculated in the double series in  $g$  and  $w$ . In the leading order (one-loop approximation) and MS scheme they read

$$Z_v = Z_h = 1 + \frac{1}{6} \frac{g}{\varepsilon}; \quad Z_{\nu_{\parallel}} = 1 - \frac{1}{2\alpha(1+\alpha)} \frac{w}{\xi} - \frac{2}{3} \frac{g}{\varepsilon}. \quad (3.13)$$

Details of the calculations can be found in Appendix B.

#### IV. RENORMALIZATION GROUP, FIXED POINTS, AND SCALING REGIMES

The relation between the initial action functional and the renormalized one  $S(\Phi, e_0) = S_R(Z_\Phi \Phi, e, \mu)$ , where  $e$  is the complete set of parameters, yields the fundamental RG differential equation whose coefficients are so-called  $\beta$  and  $\gamma$  functions (also referred to as RG functions). They are defined as

$$\beta_q = \widetilde{\mathcal{D}}_\mu q, \quad \gamma_F = \widetilde{\mathcal{D}}_\mu \ln Z_F \quad (4.1)$$

and have a deep physical meaning:  $\beta$  functions are responsible for attractive fixed points of the system that govern the sought-for asymptotic behavior while  $\gamma$  functions (also known as anomalous dimensions) give us corrections to canonical dimensions in obtained scaling regimes.

Here  $F$  denotes any quantity with nontrivial renormalization constant  $Z_F$ ,  $\widetilde{\mathcal{D}}_\mu$  is a partial derivative  $\widetilde{\mathcal{D}}_\mu = \mu \partial_\mu$  with fixed bare parameters  $\nu_{\parallel 0}$ ,  $\nu_{\perp 0}$ ,  $w_0$ ,  $g_0$ ,  $\alpha_0$ , and  $q = \{g, w, \alpha\}$  is any of the three coupling constants.

One of the basic statements of the RG theory is that the large scale asymptotic behavior of the model with respect to spatial and time scales is governed by IR attractive fixed points  $\{g^*, w^*, \alpha^*\}$  which can be found from the requirements

$$\beta_g(g^*, w^*, \alpha^*) = 0, \quad \beta_w(g^*, w^*, \alpha^*) = 0, \quad \beta_\alpha(g^*, w^*, \alpha^*) = 0. \quad (4.2)$$

The fixed point is IR attractive (or stable) if real parts of the eigenvalues  $\lambda_i$  of the matrix

$$\Omega_{ij} = \left. \frac{\partial \beta_i}{\partial g_j} \right|_{g^*, w^*, \alpha^*} \quad (4.3)$$

are positive.

This fact being the cornerstone for the theory of critical behavior is a consequence of the evolution differential equations for invariant charges:

$$\widetilde{\mathcal{D}}_{k/\mu} \bar{q}_i = \beta_i(\bar{q}_j), \quad (4.4)$$

whose solution as  $k/\mu \rightarrow 0$  (IR limit) reads

$$\bar{q}_i(k/\mu, q^*) \cong q_i^* + \text{const} \times (k/\mu)^{\lambda_i}. \quad (4.5)$$

Here  $\lambda_i$  are eigenvalues of the matrix (4.3) and  $q$  is the set of three coupling constants.

After fixed points are found from Eq. (4.2), expression (4.4) may be used for numerical simulation of RG flow. Such simulation allows one to check the obtained results. We will do it for Model 2: since it has interesting and surprising set of IR attractive fixed points, it is very desirable to compare the results of the performed analysis with the results of a different technique.

##### A. Model 1: the model with the white noise

As there is only one nontrivial independent renormalization constant in Model 1, all  $\beta$  functions for this theory can be expressed through the anomalous dimension  $\gamma_{\nu_{\parallel}}$ :

$$\beta_w = -w (\xi + \eta - \gamma_{\nu_{\parallel}}), \quad \beta_g = -g \left( \varepsilon - \frac{3}{2} \gamma_{\nu_{\parallel}} \right), \quad \beta_\alpha = -\alpha \eta. \quad (4.6)$$

From Eq. (3.7) it follows that

$$\gamma_{\nu_{\parallel}} = \frac{w}{2\alpha(1+\alpha)} + \frac{3g}{16} \quad (4.7)$$



with corrections of higher orders in  $g$  and  $w$  implied. This leads to a following system of  $\beta$  functions:

$$\begin{aligned}\beta_w &= w \left[ -\xi - \eta + \frac{w}{2\alpha(1+\alpha)} + \frac{3g}{16} \right]; \\ \beta_g &= g \left[ -\varepsilon + \frac{3w}{4\alpha(1+\alpha)} + \frac{9g}{32} \right]; \\ \beta_\alpha &= -\alpha\eta.\end{aligned}\tag{4.8}$$

It should be noted that  $\beta$  functions  $\beta_g$  and  $\beta_w$  in Eq. (4.6) satisfy the exact relation

$$w\beta_g - 3g\beta_w/2 = gw[-\varepsilon + 3(\xi + \eta)/2]\tag{4.9}$$

which is a consequence of the fact that both of them involve the same anomalous dimension  $\gamma_{v_\eta}$ . Thus, the equations (4.2) are not satisfied for arbitrary values of the exponents  $\varepsilon$ ,  $\xi$ , and  $\eta$  unless one of the coordinates  $g^*$  or  $w^*$  is equal to zero (cf. [91] for the isotropic case).

The analysis of the system (4.8) reveals two groups of the fixed points arranged according to the value of  $\alpha^*$ . The two possible values of  $\alpha^*$  are  $\alpha^* = 0$  and  $\alpha^* \rightarrow \infty$ . Let us start with the latter:  $\alpha^* = 0$ ,  $\lambda_\alpha = -\eta$ . This value of parameter  $\alpha$  corresponds to the physical system where the velocity field is frozen (or ‘‘quenched’’), see remark below Eq. (1.9).

It is necessary to replace the coupling constant  $w$  with the new one  $w' = w/\alpha$  with corresponding  $\beta$  function:

$$\beta_{w'} = \frac{\beta_w}{\alpha} - w \frac{\beta_\alpha}{\alpha^2} = w' \left( -\xi + \frac{w'}{2} + \frac{3g}{16} \right)\tag{4.10}$$

which remains nonzero at  $\alpha \rightarrow 0$ .

The relation (4.9), therefore, reads

$$w' \beta_g - 3g\beta_{w'}/2 = gw'(-\varepsilon + 3\xi/2),\tag{4.11}$$

and the system (4.8) with the replacement (4.10) allows three possible solutions:

The point (1a) with coordinates  $w'^* = 0$ ,  $g^* = 0$  and eigenvalues of matrix (4.3)  $\lambda_1 = -\varepsilon$ ,  $\lambda_2 = -\xi$ . This point is trivial, i.e., all interactions are irrelevant and no scaling is expected. It is IR attractive for  $\varepsilon < 0$ ,  $\eta < 0$ , and  $\xi < 0$ .

The point (2a) with coordinates  $w'^* = 0$ ,  $g^* = 32\varepsilon/9$ ; the corresponding eigenvalues are  $\lambda_1 = 2\varepsilon/3 - \xi$  and  $\lambda_2 = \varepsilon$ . This point is IR attractive in the area  $\eta < 0$ ,  $\varepsilon > 0$ ,  $\xi < 2\varepsilon/3$ . Since  $w^* = 0$ , turbulent motion of the environment is irrelevant in this regime and IR behavior of the model is completely defined by universality class of the original Hwa-Kardar model (1.1).

The point (3a) with coordinates  $w'^* = 2\xi$ ,  $g^* = 0$ ; the corresponding eigenvalues are  $\lambda_1 = 3\xi/2 - \varepsilon$  and  $\lambda_2 = \xi$ . This point is IR attractive when  $\eta < 0$ ,  $\xi > 0$ ,  $\xi > 2\varepsilon/3$ . Since  $g^* = 0$ , the nonlinear term in equation (1.1) is IR irrelevant in the sense of Wilson and does not affect the leading terms of the IR asymptotic behavior.

It is left to note that functions  $\beta_g$  and  $\beta_{w'}$  are proportional when  $\xi = 2\varepsilon/3$ . It leads to straight line of the fixed points on the plane  $(g, w')$ . This line is no more than a degenerate fixed point with both  $g^* \neq 0$  and  $w'^* \neq 0$ : since  $\beta_g$  and  $\beta_{w'}$  are proportional to each other, we do not have enough independent equations to solve the system (4.8) and identify the unique combination of  $g^*$  and  $w'^*$ . The zero eigenvalue along this line corresponds to zero velocity of the RG flow in this direction.

At the end of this subsection let us analyze the case of  $\alpha^* \rightarrow \infty$ . The velocity field corresponds now to the rapid-change ensemble, i.e., the ensemble with vanishing correlation time; see remark below Eq. (1.9). As before, we should pass to the new variables which are finite when  $\alpha \rightarrow \infty$ : let us introduce  $x = 1/\alpha$  and  $w'' = w/\alpha^2$ . The corresponding  $\beta$  functions are

$$\begin{aligned}\beta_x &= x\eta; \\ \beta_{w''} &= w'' \left( -\xi + \eta + \frac{w''}{2} + \frac{3}{16}g \right).\end{aligned}\tag{4.12}$$

Thus, the fixed points has coordinate  $x^* = 0$  and corresponding eigenvalue  $\lambda_x = \eta$ . IR attractive fixed points should satisfy condition  $\eta > 0$ . From Eq. (4.12) it follows that the set of the fixed points (1b), (2b), and (3b) at  $x^* = 0$  is completely the same as the set (1a), (2a), and (3a) for  $\alpha^* = 0$  after the replacement  $\xi \rightarrow \xi - \eta$  is made in the previously obtained answers. The relation similar to Eq. (4.9) is also true, thus, there is a straight line of fixed points for the case  $x^* = 0$  too. The corresponding condition reads  $\xi - \eta = 2\varepsilon/3$ .

Lastly, a case  $\eta = 0$  has to be considered. When  $\eta = 0$ , the function  $\beta_\alpha$  vanish for any given  $\alpha$  along with the corresponding eigenvalue  $\lambda_\alpha$ . The nontrivial fixed point still exist if  $\xi = 2\varepsilon/3$ . In this case it is determined by the condition  $\gamma_{v_\eta}^* = \xi$ , see Eqs. (4.7) and (4.8). Herewith, the parameters  $g^*$ ,  $w^*$  and  $\alpha^*$  can not be determined independently.

The Kolmogorov values of the exponents  $\xi = 8/3$ ,  $\eta = 4/3$  lie either in the stability region of the fixed point (2b) (universality class of the Hwa-Kardar model) or in the stability region of the fixed point (3b) (universality class of the rapid change ensemble) depending on whether  $\varepsilon$  is bigger or smaller than 2, respectively. This means, that if  $d \geq 3$ , the point (3b) corresponds to the Kolmogorov values; if  $d = 2$ , Kolmogorov values lie on the borderline between two regions.

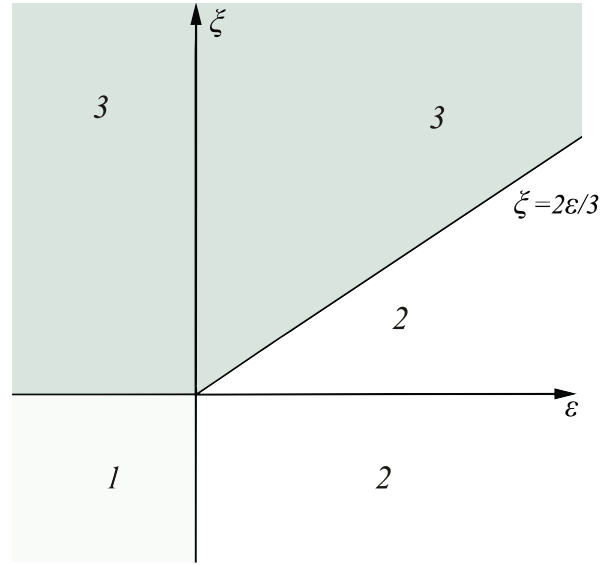


FIG. 1. Regions of stability of the fixed points for Model 1 at  $\alpha^* = 0$  in the plane  $(\varepsilon, \xi)$ . Different areas correspond to the values of the parameters for which (1a), (2a), or (3a) are IR attractive.

### B. Model 2: the model with the spatially quenched noise

There are more independent renormalization constants in Model 2 than in Model 1. Thus,  $\beta$  functions now read

$$\beta_w = -w(\xi + \eta + \gamma_w), \quad \beta_g = -g(\tilde{\varepsilon} + \gamma_g), \quad \beta_\alpha = -\alpha\eta. \quad (4.13)$$

From Eqs. (3.12) and (3.13) it follows that in one-loop approximation  $\gamma$  functions in Model 2 read

$$\gamma_w = -\frac{w}{2\alpha(1+\alpha)} - g, \quad \gamma_g = -\frac{3w}{4\alpha(1+\alpha)} - \frac{4g}{3}. \quad (4.14)$$

As a result, the system of  $\beta$  functions similar to (4.8) now takes the form

$$\begin{aligned} \beta_w &= w \left[ -\xi - \eta + \frac{w}{2\alpha(1+\alpha)} + g \right]; \\ \beta_g &= g \left[ -\tilde{\varepsilon} + \frac{3w}{4\alpha(1+\alpha)} + \frac{4g}{3} \right]; \\ \beta_\alpha &= -\alpha\eta. \end{aligned} \quad (4.15)$$

This point in the study is the most intriguing one in the whole problem: till now two models under consideration looked very similar to each other. They have the same number of coupling constants; their divergent Green functions are a bit different, but all of them are present in the initial actions requiring no new terms to be added; the models have different values of logarithmic dimensions but it is possible to perform RG analysis near the corresponding logarithmic dimension and then return to physical value by appropriate choice of  $\varepsilon$  or  $\tilde{\varepsilon}$ . Even the set of  $\beta$  functions (4.15) looks very similar to the set (4.8)! But analysis of expressions (4.15) leads to completely different fixed points than the ones we obtained in the previous subsection.

Let us discuss these fixed points. As previously, there are two possibilities for parameter  $\alpha$ :  $\alpha^* = 0$  and  $\alpha^* \rightarrow \infty$ . The first case is IR attractive if  $\eta < 0$ , the second one is IR attractive if  $\eta > 0$ . In this sense, the situation is completely the same as for Model 1 including the needed substitution  $\xi \rightarrow \xi - \eta$  in answers. Therefore, we will consider in detail only one case, that is, the case when  $\alpha^* = 0$ .

After the corresponding replacement  $w' \rightarrow w/\alpha$  the new  $\beta$  function reads

$$\beta_{w'} = w' \left( -\xi + \frac{w'}{2} + g \right) \quad (4.16)$$

and system (4.15) – (4.16) possess four different solutions. The points (1a), (2a), and (3a) correspond to similar cases in Model 1; the point (4a) is completely new.

The point (1a) has coordinates  $w^* = 0, g^* = 0$ . The eigenvalues of matrix (4.3) are  $\lambda_1 = -\tilde{\varepsilon}, \lambda_2 = -\xi$ . The point is trivial and it is IR attractive when  $\tilde{\varepsilon} < 0, \eta < 0, \xi < 0$ .

The point (2a) has coordinates  $w^* = 0, g^* = 3\tilde{\varepsilon}/4$ . The corresponding eigenvalues are  $\lambda_1 = 3\tilde{\varepsilon}/4 - \xi$  and  $\lambda_2 = \tilde{\varepsilon}$ . The point is related to the universality class of Hwa-Kardar model without turbulent advection and it is IR attractive when  $\eta < 0, \tilde{\varepsilon} > 0, \xi < 3\tilde{\varepsilon}/4$ .

The point (3a) has coordinates  $w^* = 2\xi, g^* = 0$ . The corresponding eigenvalues are  $\lambda_1 = 3\xi/2 - \tilde{\varepsilon}$  and  $\lambda_2 = \xi$ . The point is related to the regime of critical behavior in which nonlinearity of the Hwa-Kardar equation is irrelevant; the point is IR attractive when  $\eta < 0, \xi > 0, \tilde{\varepsilon} < 3\xi/2$ .

The completely new point (4a) has coordinates

$$w^* = 12\tilde{\varepsilon} - 16\xi, \quad g^* = 9\xi - 6\tilde{\varepsilon}. \quad (4.17)$$

Its eigenvalues read

$$\lambda_{1,2} = -\tilde{\varepsilon} + 2\xi \pm \sqrt{-5\tilde{\varepsilon}^2 + 13\xi\tilde{\varepsilon} - 8\xi^2}. \quad (4.18)$$

The analysis of Eqs. (4.18) reveals two possible cases: the square root is either fully real (the case A) or complex with both real and imaginary parts (the case B). The presence of imaginary parts in eigenvalues means that if this point is IR attractive (i.e., the real parts of the eigenvalues are positive), it is a spiral attractor instead of a simple node attractor.

The case A corresponds to the two areas of the values of the system parameters:  $\tilde{\varepsilon} > 0, 5\tilde{\varepsilon}/8 < \xi < 2\tilde{\varepsilon}/3$  and  $\tilde{\varepsilon} > 0, 3\tilde{\varepsilon}/4 < \xi < \tilde{\varepsilon}$ . The case B also corresponds to the two areas:  $\tilde{\varepsilon} > 0, \tilde{\varepsilon}/2 < \xi < 5\tilde{\varepsilon}/8$  and the large area which is parameterized by conditions  $\tilde{\varepsilon} > 0, \xi > \tilde{\varepsilon}$  and  $\tilde{\varepsilon} < 0, \xi > \tilde{\varepsilon}/2$ . It is very interesting that we see a gap in the region of stability of these points; moreover, it is intriguing that the area related to the node attractor lies “inside” the area of spiral attractor.

Another surprising fact is that the borders of the gap in the stability region of the point (4a) completely coincide with the upper and lower borders of stability regions of the points (2a) and (3a) which are defined by their own (independent) eigenvalues! It is also very interesting that even the gap of the point (4a) is a stability region of two fixed points.

Moreover, stability region of one of the nontrivial fixed points lies in the area  $\tilde{\varepsilon} < 0, \xi < 0$ . We have never before met a system with such a feature.

The general pattern of stability is shown in Fig. 2. The straight lines denote borders of the stability regions (areas where the points are IR attractive); the white color and different types of grey color simplify the visual perception of the picture. The subscripts “R” and “C” near the point (4) denote the type of the root in Eqs. (4.18) and, therefore, the type of the attractor. Designation  $4^R$  corresponds to the node attractor, designation  $4^C$  corresponds to the spiral attractor. The points (1), (2), and (3) do not have such variants and, therefore, have no subscripts.

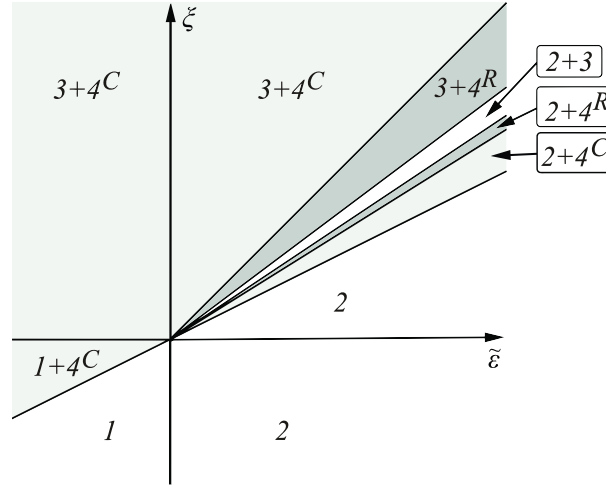


FIG. 2. Regions of stability of the fixed points for Model 2 at  $\alpha^* = 0$  in the plane  $(\tilde{\varepsilon}, \xi)$ . Different areas correspond to the values of the parameters for which points (1a), (2a), (3a), or (4a) are IR attractive.

The main reason for this dramatic difference between the results obtained for Model 1 and for Model 2 is the absence of the relation such as (4.9) in Model 2. This is, in its turn, a consequence of there being more than one independent renormalization constant  $Z$  in the model. It opens the possibility for a fixed point with both  $g^* \neq 0$  and  $w^* \neq 0$  to exist. Therefore, it was natural to expect the set of fixed points in Model 2 to be more interesting and rich than the set in Model 1. Nevertheless, one could hardly expect the obtained picture of fixed points to be so complicated and to consist of points with overlapping stability regions

that even have gaps in them<sup>3</sup>. This result is really surprising; nothing at the start of the analysis of the system (4.15) indicated that the result was to be expected.

Overlaps between the stability regions of different fixed points have important implication for the universality of system's asymptotic behavior. Universality means that the behavior depends only on the global characteristics of the system like spatial dimension  $d$  and values of  $\xi$  and  $\eta$ . But if several fixed points share a stability region, then the RG flow may reach either one of them depending on the initial values of the coupling constants. This dependence can be interpreted as a loss of universality (universality violation).

While Kolmogorov values of the exponents are  $\xi = 8/3$ ,  $\eta = 4/3$ , the stability region corresponding to them formally depends on the value of  $\tilde{\varepsilon}$ . As such, the Kolmogorov values may relate to either of the following regions: the area where both fixed points (3b) and (4b) are IR attractive, the area where both (2b) and (3b) are IR attractive, the area where both (2b) and (4b) are IR attractive, or the area where only (2b) is IR attractive. However, at  $\eta = 4/3$  the wedges in Fig. 2 are very small and most of the regions are unattainable for integer values of  $d$ . The result of this is that for every  $\tilde{\varepsilon} > 8/3$ , i.e., for  $d \leq 3$ , the Kolmogorov values belong to the stability region of the fixed point (2b). If  $\tilde{\varepsilon} = 2$ , i.e., if  $d = 4$ , the Kolmogorov values lie on the borderline between two regions: the region where both fixed points (2b) and (4b) are IR attractive and the region where both points (2b) and (3b) are IR attractive. Note, that for another value of  $\eta$  the Kolmogorov values may belong to any of the other regions.

Since the obtained results look so complicated, we used expressions (4.4) as dynamical equations for numerical simulation of RG flow. The arrows on the lines show direction towards the IR limit, i.e., the limit  $k/\mu \rightarrow 0$ . We carefully checked each stability region and obtained full agreement with theoretical analysis. Below one of the figures is attached.

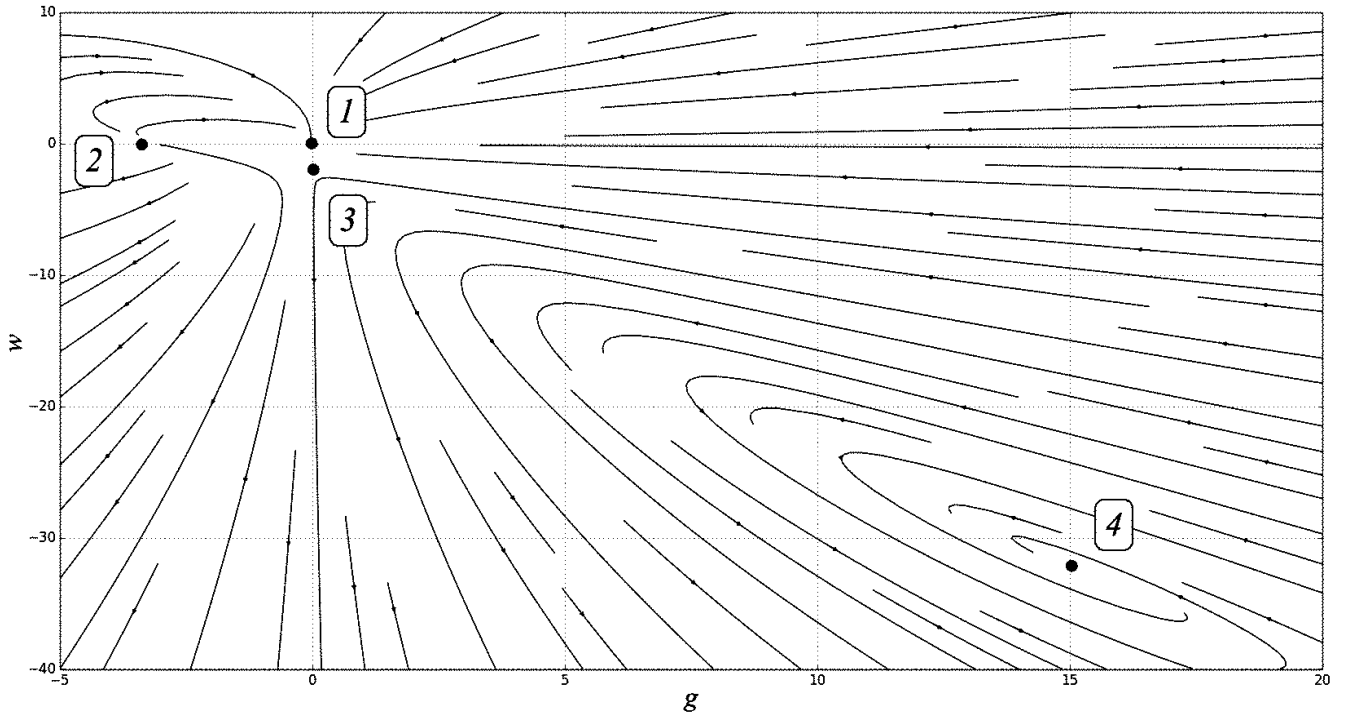


FIG. 3. RG flow in Model 2 for  $\alpha = 0$ ,  $\tilde{\varepsilon} = -4$ ,  $\xi = -1$ . The numbers indicate the fixed points (1a), (2a), (3a), and (4a). The fixed point (1a) is a nod attractor while the fixed point (4a) is a spiral attractor.

## V. CRITICAL SCALING AND CRITICAL DIMENSIONS.

The renormalized Green functions  $G^R$  satisfy RG equation in the leading order of IR asymptotic behavior when the substitution  $q \rightarrow q^*$  is made. This is a consequence of expressions (4.5);  $q$  is the set of three coupling constants. As a result, the RG equation

<sup>3</sup> It is important to note that not only stability region of the “new” point 4 intersects with the regions of other fixed points but that there are also overlaps between stability regions of the points 2 and 3. In Model 1 stability regions of the similar points have no such overlaps.

reads

$$\left( \mathcal{D}_\mu - \sum_i \gamma_i^* \mathcal{D}_i + \sum_\Phi N_\Phi \gamma_\Phi^* \right) G^R = 0, \quad (5.1)$$

where  $\gamma_\Phi$  and  $\gamma_i$  are anomalous dimensions of the fields and the parameters that require renormalization, respectively. Since values of anomalous dimensions at fixed point  $\gamma_\Phi^*$  and  $\gamma_i^*$  are constants, equation (5.1) is a differential equation with constant coefficients and, therefore, is an equation of the same type as differential equations for canonical scale invariance. Solution of the system of equations that includes Eq. (5.1) together with the equations for canonical scale invariance gives us critical dimension  $\Delta_F$  of an IR relevant quantity  $F$  (a field or a parameter), see [14]. Since we have two spatial (momentum) scales while for both models renormalization constants  $Z_{v_\parallel} \neq 0$  and  $Z_{v_\perp} = 1$ , this dimension reads [67, 86]

$$\Delta_F = d_F^\perp + \Delta_\parallel d_F^\parallel + 2d_F^\omega + \gamma_F^*; \quad \Delta_\parallel = 1 + \gamma_{v_\parallel}^*/2. \quad (5.2)$$

The factor 1/2 in expression for  $\Delta_\parallel$  is due to canonical dimension  $d_{v_\parallel}^\parallel = -2$ ; since  $\gamma_{v_\perp} = 0$ , the critical dimension of the frequency  $\Delta_\omega$  is simply equal to 2:  $\Delta_\omega = 2$ . As usual,  $d_F$  are canonical dimensions (see Tables I and II) and  $\gamma_F^*$  is corresponding anomalous dimension taken at the fixed point. The normalization condition  $\Delta_\perp = 1$  is used.

Depending on the values of  $\eta$ ,  $\xi$ , and  $\varepsilon$  or  $\tilde{\varepsilon}$ , RG flow reaches certain fixed point. Substitution of the fixed point coordinates ( $g^*$ ,  $w^*$  and  $\alpha^*$ ) into Eqs. (5.2) leads to answers for critical dimensions that correspond to the possible scaling regimes of the system.

Calculation of critical dimensions is the final goal of the general scheme: they appear in the pair correlation function of the field  $h$  in the following way

$$\langle h(t, \mathbf{x}) h(0, \mathbf{0}) \rangle \simeq r_\perp^{-2\Delta_h} \mathcal{F} \left( t/r_\perp^{\Delta_\omega}, r_\parallel/r_\perp^{\Delta_\parallel} \right) \quad (5.3)$$

and allow direct comparison with experiments. Here  $r_\perp = |\mathbf{x}_\perp|$ ,  $r_\parallel = x_\parallel$ , and  $\mathcal{F}$  is a scaling function of critically dimensionless arguments.

### A. Model 1: the model with the white noise

The functions  $\beta_g$  and  $\beta_w$  involve the same anomalous dimension  $\gamma_{v_\parallel}$  [see relation (4.9)] in Model 1, so the value of  $\gamma_{v_\parallel}^*$  and the critical dimensions are found exactly despite the fact that coordinates of the fixed points are found only in one-loop approximation. This nontrivial fact reminds of a similar observation in the stochastic NS equation [102] – [104], where all the anomalous dimensions can be found exactly without any practical calculation of the renormalization constants. Indeed, if one of the coupling constants (say,  $w$ ) is necessary equal to zero at fixed point, it follows from Eqs. (4.6) that  $\gamma_{v_\parallel}^* = 2\varepsilon/3$ . Since Eqs. (4.6) follow directly from the definitions of  $\beta$  and  $\gamma$  functions, they are exact. Therefore, the value of  $\gamma_{v_\parallel}^*$  obtained above is also exact. Nevertheless, it is necessary to calculate Feynman graphs to check the stability regions of different fixed points (i.e., to find the derivatives of  $\beta$  functions at fixed points).

Critical dimensions for the trivial points (1a) and (1b) coincide with each other and read

$$\Delta_{h'} = d - 1 = 3 - \varepsilon, \quad \Delta_h = \Delta_v = 1. \quad (5.4)$$

Critical dimensions for the fixed points (2a) and (2b) read

$$\Delta_{h'} = 3 - \frac{\varepsilon}{3}, \quad \Delta_h = \Delta_v = 1 - \frac{\varepsilon}{3}. \quad (5.5)$$

Critical dimensions for the fixed points (3a) and (3b) are not the same and read

$$\Delta_{h'} = 3 - \varepsilon + \xi, \quad \Delta_h = \Delta_v = 1 - \frac{\xi}{2} \quad \text{for the point (3a);} \quad (5.6)$$

$$\Delta_{h'} = 3 - \varepsilon + \xi - \eta, \quad \Delta_h = \Delta_v = 1 - \frac{\xi - \eta}{2} \quad \text{for the point (3b).} \quad (5.7)$$

As it should be, the results for the fixed point (2b) agree with those obtained in [37]<sup>4</sup>. The results for all three points (1b), (2b), and (3b) that correspond to the rapid-change velocity ensemble agree with those obtained in [70]<sup>5</sup>.

<sup>4</sup> One has to identify  $z = \Delta_\omega/\Delta_\parallel$ ,  $\zeta = 1/\Delta_\parallel$ , and  $\chi = -\Delta_h/\Delta_\parallel$ .

<sup>5</sup> One has to identify  $\xi$  from [70] with  $\xi - \eta$  in Eqs. (5.7); moreover, there are misprints in [70] in answers for  $\Delta_{h'}$ .

### B. Model 2: the model with the spatially quenched noise

In Model 2 there is no exact relation between  $\beta_g$  and  $\beta_w$ ; therefore, all of the results (both coordinates of the fixed points and the critical dimensions) imply corrections in  $\tilde{\epsilon}$ ,  $\xi$  and  $\eta$  of second order and higher (except the critical dimensions for the points (3a) and (3b), see below). Moreover, since the fields  $h$ ,  $h'$ , and  $v$  have nontrivial renormalization constants, now we should take into account corresponding anomalous dimensions. From Eqs. (3.12) and (3.13) it follows that they read

$$\gamma_h = \gamma_v = -\frac{g}{6}, \quad \gamma_{h'} = \frac{g}{6}. \quad (5.8)$$

Critical dimensions for the trivial points (1a) and (1b) are still very simple and read

$$\Delta_{h'} = 5 - \tilde{\epsilon}, \quad \Delta_h = \Delta_v = 1. \quad (5.9)$$

Critical dimensions for the points (2a) and (2b) are

$$\Delta_{h'} = 5 - \frac{3\tilde{\epsilon}}{8}, \quad \Delta_h = \Delta_v = 1 - \frac{3\tilde{\epsilon}}{8}. \quad (5.10)$$

Since the differences between Eqs. (4.15) (for Model 2) and Eqs. (4.8) (for Model 1) are presented only in the parts that contain the coupling constant  $g$ , the coordinates of the fixed points (3a) and (3b) (which satisfy the case  $g^* = 0$ ) coincide for both models. Owing to this fact and Eqs. (5.8), the only difference in the critical dimensions for the points (3) in both models is due to their canonical parts which are connected with the logarithmic dimensions  $d = 6$  for Model 2 and  $d = 4$  for Model 1.

Thus, the critical dimensions for the points (3a) and (3b) are

$$\Delta_{h'} = 5 - \tilde{\epsilon} + \xi, \quad \Delta_h = \Delta_v = 1 - \frac{\xi}{2} \quad \text{for the point (3a);} \quad (5.11)$$

$$\Delta_{h'} = 5 - \tilde{\epsilon} + \xi - \eta, \quad \Delta_h = \Delta_v = 1 - \frac{\xi - \eta}{2} \quad \text{for the point (3b).} \quad (5.12)$$

These results are exact, see Appendix B.

The critical dimensions for the fully nontrivial points (4a) and (4b) read

$$\Delta_{h'} = 5 - \frac{\xi}{2}, \quad \Delta_h = \Delta_v = 1 - \frac{\xi}{2} \quad \text{for the point (4a);} \quad (5.13)$$

$$\Delta_{h'} = 5 - \frac{\xi - \eta}{2}, \quad \Delta_h = \Delta_v = 1 - \frac{\xi - \eta}{2} \quad \text{for the point (4b).} \quad (5.14)$$

From Eqs. (5.11) – (5.14) it follows that critical dimensions for the fields  $h$  and  $v$  coincide with each other for the fixed points (3) and (4). This coincidence looks intriguing for two reasons: the answers for the fixed points (3) are exact while the answers for the point (4) imply corrections of orders  $\xi^2$ ,  $\eta^2$ , etc. The second point is that, in contrast with the coincidence of critical dimensions for the point (3) in two models, the algebraic expressions which leads to the same answers for points (3) and (4) in Model 2 are completely different. Therefore, this equality between critical dimensions at different points may be both just an artifact of one-loop approximation and some law with nontrivial underlying physics. To clarify this situation it is necessary to go beyond one-loop approximation and to check whether the same coincidence is true in the next orders or not. This is one of the possible tasks for the future.

## VI. CONCLUSION

In this paper we applied field theoretic renormalization group to the two models of statistical physics. The first model is described by the stochastic Hwa-Kardar equation for self-organized criticality with the white noise as a random force; in the second model time-independent (spatially quenched) noise was used. Both models took into account turbulent motion of the environment described by some statistical ensemble.

The measurable and, therefore, sought-for quantities are critical dimensions of the fields, which are connected to exponents of correlation and structure functions. These dimensions are defined by infrared attractive fixed points in the renormalization group approach, so the main goal of the paper is to find the sets of fixed points for both models.

Our analysis shows that despite the fact that both models are very similar to each other even in the obtained expressions for the  $\beta$  functions, the final pictures of fixed points are completely different. If for the model with the white noise the obtained picture is more or less typical, i.e., there are three fixed points with no gaps or overlaps between their stability regions, the picture for the model with the spatially quenched noise seems to be much more complicated. It contains overlaps between regions of stability of different fixed points, and, from the physical point of view, this feature may be interpreted as a loss of universality: now the

critical dimensions depend not only on global characteristic of the system like space dimension  $d$  and values of  $\xi$  and  $\eta$  which characterise velocity field, but also on the initial values of the coupling constants. These initial conditions determine which of the possible fixed points is reached by the RG flow.

It is interesting that spatially quenched noise is widely used in various models but does not lead to such complicated behavior as a rule. Moreover, the stochastic Hwa-Kardar equation with the spatially quenched noise but without turbulent field  $v$  does not display such interesting properties as we see here [46]. Therefore, the obtained picture is a consequence of the influence of both type of the noise and presence of the velocity field in the model. For this reason it would be interesting to consider the same model with the velocity described not by some statistical ensemble, but by the nonlinear Navier-Stokes equation. In this case the system will obtain one more viscosity coefficient and one more field, namely response field  $v'$ , and we may expect more interesting behavior. Or, perhaps, we will obtain more common picture and will conclude that the intriguing results which we see here are nothing more than some accidental feature in one of the models. In any case, it would be very interesting to understand which part of the formulation of the problem under consideration is responsible for such complicated behavior.

Other implications of our analysis seem to be more predictable. Despite the fact that we used velocity ensemble with finite correlation time for modeling of turbulent environment, the possible nontrivial types of the IR behavior appear to be reduced to only two cases: the rapid-change type behavior and the frozen (time-independent) behavior. This fact is not surprising because such a feature has been observed in many different systems before; see, e.g., [56, 57, 86, 88, 90, 93] and review paper [101].

Second easily explicable fact is that the model with the white noise possess only three IR attractive fixed points with always at least one coupling constant equal to zero while the model with the spatially quenched noise involves four IR attractive fixed points including the one for which both couplings are nontrivial. An interesting aspect in this connection is that critical dimensions of the fields  $h$  and  $v$  (but not  $h'$ ) are equal in the fully nontrivial regime presented only in the model with the spatially quenched noise and in one of the trivial regimes which we also see in the model with the white noise. This is really surprising and may be both an artifact of one-loop approximation which we used and some law with nontrivial underlying physics. To clarify this situation it is necessary to go beyond one-loop approximation. This is also one of the possible tasks for the future.

## ACKNOWLEDGMENTS

The reported study was funded by RFBR, project number 20-32-70139. The work by N. V. Antonov and P. I. Kakin was also supported by the Foundation for the Advancement of Theoretical Physics and Mathematics ‘‘BASIS.’’

## Appendix A: Model 1: calculation details

This section contains detailed calculations of the diagrams defining the renormalization constant  $Z_{v_{\parallel}}$  (see Sec. III A). All calculations are performed in the analytical regularization and MS (minimal subtraction) scheme.

Since this model we deal with involves only one divergent function  $\langle h'h \rangle_{1-ir}$ , there are only two one-loop graphs needed to be calculated:

$$D_1 = \text{---} \overbrace{\text{---}}^{\text{---}} \text{---} \quad \text{and} \quad D_2 = \text{---} \overbrace{\text{---}}^{\text{---}} \text{---} . \quad (\text{A1})$$

Here and below the straight line corresponds to the field  $h$ , the dashed line corresponds to the field  $h'$ , and the wave line corresponds to the velocity field  $v$ . The propagator functions and vertices are defined in Sec. II A.

Let us start with the graph  $D_1$ . Analytical expression for it reads

$$D_1 = -2\pi B_0 \int \frac{d\omega}{2\pi} \frac{d^d \mathbf{k}}{(2\pi)^d} \delta(k_{\parallel}) \frac{k_{\perp}^{5-d-(\xi+\eta)}}{\omega^2 + (\alpha_0 v_{\perp 0} k_{\perp}^{2-\eta})^2} \frac{p_{\parallel}(p_{\parallel} - k_{\parallel})}{-i\omega + \epsilon(p - k)}, \quad (\text{A2})$$

where  $\epsilon(k)$  is denoted in Eq. (2.4),  $\mathbf{p}$  is an external momenta, and  $p_{\parallel} = (\mathbf{p} \cdot \mathbf{n})$ . Since  $d_{\Gamma} = 2$  for this function, we are looking for the term proportional to  $p_{\parallel}^2$ . Owing to this fact, after trivial integration over  $k_{\parallel}$  and after integration over the frequency  $\omega$  one obtains

$$D_1 = -B_0 p_{\parallel}^2 \frac{1}{2\alpha_0 v_{\perp 0}^2} \int_{k_{\perp} > m} \frac{d^{d-1} \mathbf{k}_{\perp}}{(2\pi)^{d-1}} \frac{k_{\perp}^{5-d-(\xi+\eta)}}{k_{\perp}^{2-\eta} (\alpha_0 k_{\perp}^{2-\eta} + k_{\perp}^2)}. \quad (\text{A3})$$

The integration over the internal momenta  $\mathbf{k}_\perp$  can be simplified in the MS scheme, in which all the anomalous dimensions are independent of the regularizers like  $\xi$  and  $\eta$ . Hence, we may choose them arbitrary with the only restriction that our diagrams have to remain UV finite [93]. The most convenient way is to put  $\eta = 0$ . Thus, after the integration one obtains

$$D_1 = -p_\parallel^2 \frac{B_0}{2\alpha_0(\alpha_0 + 1)v_{\perp_0}^2} \frac{S_{d-1}}{(2\pi)^{d-1}} \frac{m^{-\xi}}{\xi}, \quad (\text{A4})$$

where  $S_{d-1}$  is the area of the unit sphere in the  $(d-1)$ -dimensional space.

The analytical expression for the graph  $D_2$  reads

$$D_2 = -D_0 \int \frac{d\omega}{2\pi} \frac{d^d \mathbf{k}}{(2\pi)^d} \frac{p_\parallel(p_\parallel - k_\parallel)}{[\omega^2 + \epsilon^2(k)][-i\omega + \epsilon(p-k)]}. \quad (\text{A5})$$

Since now we do not have  $\delta(k_\parallel)$  in our integrand, expansion of expression (A5) over  $p_\parallel$  gives us two terms. First one referred to as  $I_1$  reads

$$I_1 = -D_0 p_\parallel^2 \int \frac{d\omega}{2\pi} \frac{d^d \mathbf{k}}{(2\pi)^d} \frac{1}{[\omega^2 + \epsilon^2(k)][-i\omega + \epsilon(k)]}. \quad (\text{A6})$$

After integration over  $\omega$  one obtains

$$I_1 = -p_\parallel^2 \frac{D_0}{4} \int \frac{d^d \mathbf{k}}{(2\pi)^d} \frac{1}{(v_{\parallel_0} k_\parallel^2 + v_{\perp_0} k_\perp^2)^2}. \quad (\text{A7})$$

To perform integration in Eq. (A7) it is convenient to pass to the new variables  $l_\parallel = v_{\parallel_0}^{1/2} k_\parallel$  and  $l_\perp = v_{\perp_0}^{(d-1)/2} k_\perp$  which absorb viscosity coefficients. Thus, expression for  $I_1$  reads

$$I_1 = -p_\parallel^2 \frac{D_0}{4v_{\parallel_0}^{1/2} v_{\perp_0}^{(d-1)/2}} \int \frac{d^d \mathbf{l}}{(2\pi)^d} \frac{1}{l^4}, \quad (\text{A8})$$

where  $l^2 = l_\parallel^2 + l_\perp^2$ . Substituting the value of the logarithmic dimension  $d = 4 - \varepsilon$  one finally obtains

$$I_1 = -p_\parallel^2 \frac{D_0}{4v_{\parallel_0}^{1/2} v_{\perp_0}^{3/2}} \frac{S_d}{(2\pi)^d} \int_{l>m} \frac{dl}{l^{1+\varepsilon}} = -p_\parallel^2 \frac{D_0}{4v_{\parallel_0}^{1/2} v_{\perp_0}^{3/2}} \frac{S_d}{(2\pi)^d} \frac{m^{-\varepsilon}}{\varepsilon}. \quad (\text{A9})$$

To write the second term in Eq. (A5) referred to as  $I_2$  we should use expansion

$$\frac{1}{\epsilon(k) + \epsilon(p-k)} = \frac{1}{2\epsilon(k)} \left[ 1 + \frac{v_{\parallel_0} p_\parallel k_\parallel + v_{\perp_0} (\mathbf{p}_\perp \cdot \mathbf{k}_\perp)}{\epsilon(k)} \right] + O(p^2). \quad (\text{A10})$$

Using the fact that only terms even in  $\mathbf{k}$  give nonzero contributions one obtains

$$I_2 = p_\parallel \frac{D_0}{4} \int \frac{d^d \mathbf{k}}{(2\pi)^d} \frac{k_\parallel [v_{\parallel_0} p_\parallel k_\parallel + v_{\perp_0} (\mathbf{p}_\perp \cdot \mathbf{k}_\perp)]}{(v_{\parallel_0} k_\parallel^2 + v_{\perp_0} k_\perp^2)^3}. \quad (\text{A11})$$

After the same replacement of the variables as the one we used in Eq. (A7) expression for  $I_2$  takes the form

$$I_2 = p_\parallel \frac{D_0}{4v_{\parallel_0}^{1/2} v_{\perp_0}^{(d-1)/2}} \int \frac{d^d \mathbf{l}}{(2\pi)^d} \frac{[p_\parallel l_\parallel^2 + l_\parallel (\mathbf{p}_\perp \cdot \mathbf{l}_\perp)]}{l^6}. \quad (\text{A12})$$

In order to integrate over the vector  $\mathbf{l}$  we need to average our expression over the angles:

$$\int d\mathbf{l} f(\mathbf{l}) = S_d \int_{l>m} dl l^{d-1} \langle f(\mathbf{l}) \rangle, \quad (\text{A13})$$

where  $\langle \dots \rangle$  is the averaging over the unit sphere in the  $d$ -dimensional space. In particular case of two indices it reads

$$\left\langle \frac{l_i l_j}{l^2} \right\rangle = \frac{\delta_{ij}}{d}. \quad (\text{A14})$$



For the second term in Eq. (A12) this gives

$$\int \frac{d^d \mathbf{l}}{(2\pi)^d} \frac{l_{\parallel}(\mathbf{p}_{\perp} \cdot \mathbf{l}_{\perp})}{l^6} = \int \frac{d^d \mathbf{l}}{(2\pi)^d} \frac{l_i n_i l_j p_{j\perp}}{l^6} = \frac{S_d}{d} \delta_{ij} n_i p_{j\perp} \int_{l>m} \frac{dl}{l^4} = 0, \quad (\text{A15})$$

where the last equality follows from the fact that  $\delta_{ij} n_i p_{j\perp} = n_j p_{j\perp} = 0$ .

The first term in Eq. (A12) is nonzero and after substitution  $d = 4 - \varepsilon$  gives

$$I_2 = p_{\parallel}^2 \frac{D_0}{4v_{\parallel 0}^{1/2} v_{\perp 0}^{3/2}} \int \frac{d^d \mathbf{l}}{(2\pi)^d} \frac{n_i n_j l_i l_j}{l^6} = p_{\parallel}^2 \frac{D_0}{16v_{\parallel 0}^{1/2} v_{\perp 0}^{3/2}} \frac{S_d}{(2\pi)^d} \frac{m^{-\varepsilon}}{\varepsilon}. \quad (\text{A16})$$

Combining together expressions for  $I_1$  and  $I_2$  one finally obtains

$$D_2 = -p_{\parallel}^2 \frac{3}{16} \frac{D_0}{v_{\parallel 0}^{1/2} v_{\perp 0}^{3/2}} \frac{S_d}{(2\pi)^d} \frac{m^{-\varepsilon}}{\varepsilon}. \quad (\text{A17})$$

The one-loop approximation for the 1-irreducible Green function  $\langle h'h \rangle_{1-ir}$  reads

$$\langle h'h \rangle_{1-ir} = i\omega - v_{\parallel 0} p_{\parallel 0}^2 - v_{\perp 0} p_{\perp 0}^2 + \Sigma, \quad (\text{A18})$$

where  $\Sigma$  is the self-energy operator and is represented by the sum of the graphs  $D_1$  and  $D_2$ . Combining this expression with answers (A4) and (A17) and taking into account definitions of the coupling constants [see Eqs. (2.5)] one immediately obtains the renormalization constants  $Z_{v_{\parallel}}$  and  $Z_{v_{\perp}}$ , see Eq. (3.7).

## Appendix B: Model 2: calculation details

This section contains detailed calculations of the diagrams defining the renormalization constants  $Z_{v_{\parallel}}$ ,  $Z_h$ , and  $Z_v$  (see Sec. III B). Since we deal with three divergent Green functions in Model 2, namely  $\langle h'h \rangle_{1-ir}$ ,  $\langle h'hv \rangle_{1-ir}$ , and  $\langle h'hh \rangle_{1-ir}$ , we have to calculate both two-tailed and three-tailed graphs.

Let us start with two-tailed graphs which enter the same expansion for function  $\langle h'h \rangle_{1-ir}$  as Eq. (A18):

$$\langle h'h \rangle_{1-ir} = i\omega - v_{\parallel 0} p_{\parallel 0}^2 - v_{\perp 0} p_{\perp 0}^2 + \Sigma. \quad (\text{B1})$$

The graphs  $\tilde{D}_1$  and  $\tilde{D}_2$ , the sum of which represents the self-energy operator  $\Sigma$  (here and below graphs with tilde denote graphs for Model 2), are depicted by the same figures as shown in Eqs. (A1). Moreover, the only difference between two models in Feynman rules is in the expression for the propagator  $\langle hh \rangle_0$  (see Sec. II B) which does not enter the expression for  $\tilde{D}_1$ . Thus,

$$\tilde{D}_1 = D_1 = -p_{\parallel}^2 \frac{B_0}{2\alpha_0(\alpha_0 + 1)v_{\perp 0}^2} \frac{S_{d-1}}{(2\pi)^{d-1}} \frac{m^{-\xi}}{\xi}. \quad (\text{B2})$$

The analytical expression for the graph  $\tilde{D}_2$  reads

$$\tilde{D}_2 = -D_0 \int \frac{d\omega}{2\pi} \frac{d^d \mathbf{k}}{(2\pi)^d} \frac{2\pi\delta(\omega)}{\varepsilon^2(k)} \frac{p_{\parallel}(p_{\parallel} - k_{\parallel})}{-i\omega + \varepsilon(p - k)}. \quad (\text{B3})$$

Integration of Eq. (B3) over the frequency is trivial and gives

$$\tilde{D}_2 = -D_0 \int \frac{d^d \mathbf{k}}{(2\pi)^d} \frac{1}{\varepsilon^2(k)} \frac{p_{\parallel}(p_{\parallel} - k_{\parallel})}{\varepsilon(p - k)}. \quad (\text{B4})$$

The general logic of the integration of expression for  $\tilde{D}_2$  is absolutely the same as in the previous section for the graph  $D_2$ , see Eqs. (A5) – (A17): we have to extract the term  $O(p^2)$  from the expression  $p_{\parallel}(p_{\parallel} - k_{\parallel})/\varepsilon(p - k)$  and then perform integration over the vector  $\mathbf{k}$  taking into account  $\tilde{\varepsilon} = 6 - d$ . Therefore, we will omit these algebraic steps and write directly an answer:

$$\tilde{D}_2 = -p_{\parallel}^2 \frac{2}{3} \frac{D_0}{v_{\parallel 0}^{1/2} v_{\perp 0}^{5/2}} \frac{S_d}{(2\pi)^d} \frac{m^{-\tilde{\varepsilon}}}{\tilde{\varepsilon}}. \quad (\text{B5})$$

By combining expressions (B2) and (B5) and substituting them into Eq. (B1) one immediately obtains the renormalization constants  $Z_{v_{\parallel}}$  and  $Z_{v_{\perp}}$ , see Eqs. (3.13).

Now let us consider the graphs that correspond to the function  $\langle h'hh \rangle_{1-ir}$ . Using our Feynman rules we may construct six graphs:

$$\begin{aligned} \tilde{D}_3 = & \text{triangle with solid lines}, \quad \tilde{D}_4 = \text{triangle with solid lines}, \quad \tilde{D}_5 = \text{triangle with solid lines}, \\ \tilde{D}_6 = & \text{triangle with wavy lines}, \quad \tilde{D}_7 = \text{triangle with wavy lines}, \quad \text{and } \tilde{D}_8 = \text{triangle with wavy lines}. \end{aligned} \quad (\text{B6})$$

Let us start with the last one, the graph  $\tilde{D}_8$ . The analytical expression for it reads

$$\tilde{D}_8 = 2\pi i^3 B_0 \int \frac{d\omega}{2\pi} \frac{d^d \mathbf{k}}{(2\pi)^d} \delta(k_{\parallel}) \frac{k_{\perp}^{5-d-(\xi+\eta)}}{\omega^2 + (\alpha_0 v_{\perp 0} k_{\perp}^{2-\eta})^2} \frac{(p_{\parallel} + q_{\parallel})(p_{\parallel} + q_{\parallel} + k_{\parallel})(k_{\parallel} + q_{\parallel})}{[-i\omega + \epsilon(p+k)][-i\omega + \epsilon(p+q+k)]}. \quad (\text{B7})$$

Here  $\mathbf{p}$  and  $\mathbf{q}$  are external momenta,  $\mathbf{k}$  is momentum of integration. Since the divergence index for this graph  $d_{\Gamma} = 1$ , we are looking for the terms proportional to  $\mathbf{p}^1$  or  $\mathbf{q}^1$ . Expression (B7) has a factor  $(p_{\parallel} + q_{\parallel})$  from the very beginning, therefore, we may immediately put  $\mathbf{p} = \mathbf{q} = 0$  in all the other coefficients. This observation together with  $\delta(k_{\parallel})$  presented in r.h.s. of Eq. (B7) leads directly to the fact that  $\tilde{D}_8 = 0$ .

The same feature is true also for the graphs  $\tilde{D}_6$  and  $\tilde{D}_7$ . The fact that divergent parts of all three graphs containing velocity propagator  $\langle vv \rangle_0$  are equal to zero leads to independence of renormalization constant  $Z_h$  from the coupling constant  $w$ . Moreover, this effect holds true in all orders of perturbation theory: in any multiloop graph of such type we may choose the same direction of momenta flow as we chose in Eq. (B7).

Despite the fact that we consider Green function  $\langle h'hh \rangle_{1-ir}$  now, let us mention in this place that the function  $\langle h'hw \rangle_{1-ir}$  does not have graphs similar to  $\tilde{D}_6 - \tilde{D}_8$ . The reason for this is that we simply do not have a vertex with two fields  $v$  in our Feynman rules. Therefore,  $Z_v$  also does not have dependence on the coupling constant  $w$  in all orders of perturbation theory.

This feature of the model has a great consequence for the critical dimensions at fixed points (3a) and (3b) which correspond to the case  $g^* = 0$ ,  $w^* \neq 0$ . Since  $\gamma_v^* = \gamma_h^* = 0$  in all orders of perturbation theory at these points, critical dimensions found in one-loop approximation [see Eqs. (5.11) – (5.12)] are, in fact, exact. The situation is similar to Model 1. The difference is that we do not have any relation like Eq. (4.9) in Model 2 from which this fact would follow obviously; moreover, critical dimensions in Model 2 are exact only for points (3a) and (3b), for all other scaling regimes they have corrections of orders  $\tilde{\epsilon}^2$ ,  $\xi^2$ ,  $\eta^2$  and higher.

Divergent parts of other three graphs are nonzero. The analytical expression for the graph  $\tilde{D}_3$  reads

$$\tilde{D}_3 = -i^3 D_0 \int \frac{d\omega}{2\pi} \frac{d^d \mathbf{k}}{(2\pi)^d} \frac{2\pi \delta(\omega)}{\epsilon^2(k)} \frac{(p_{\parallel} + q_{\parallel})(p_{\parallel} + q_{\parallel} + k_{\parallel})(k_{\parallel} + q_{\parallel})}{[-i\omega + \epsilon(p+k)][-i\omega + \epsilon(p+q+k)]}. \quad (\text{B8})$$

After trivial integration over the frequency  $\omega$ , the term proportional to  $(p_{\parallel} + q_{\parallel})$  takes the form

$$\tilde{D}_3 = i(p_{\parallel} + q_{\parallel}) D_0 \int \frac{d^d \mathbf{k}}{(2\pi)^d} \frac{k_{\parallel}^2}{\epsilon^4(k)}. \quad (\text{B9})$$

Using the same techniques as we described above, from Eq. (B9) one immediately obtains an answer:

$$\tilde{D}_3 = i(p_{\parallel} + q_{\parallel}) \frac{1}{6} \frac{D_0}{v_{\parallel 0}^{1/2} v_{\perp 0}^{5/2}} \frac{S_d}{(2\pi)^d} \frac{m^{-\tilde{\epsilon}}}{\tilde{\epsilon}}. \quad (\text{B10})$$

The graphs  $\tilde{D}_4$  and  $\tilde{D}_5$  are equal to each other and differ from  $\tilde{D}_3$  only by the sign. Thus,

$$\tilde{D}_4 = \tilde{D}_5 = -i(p_{\parallel} + q_{\parallel}) \frac{1}{6} \frac{D_0}{v_{\parallel}^{1/2} v_{\perp}^{5/2}} \frac{S_d}{(2\pi)^d} \frac{m^{-\tilde{\epsilon}}}{\tilde{\epsilon}}. \quad (\text{B11})$$

All of the graphs  $\tilde{D}_1 - \tilde{D}_8$  have the same symmetry coefficient equal to unity.

The one-loop approximation for the 1-irreducible Green function  $\langle h'hh \rangle_{1-ir}$  reads

$$\langle h'hh \rangle_{1-ir} = V_{h'hh} + \tilde{D}_3 + \tilde{D}_4 + \tilde{D}_5. \quad (\text{B12})$$

From Eqs. (B10) – (B12) one immediately obtains an answer for renormalization constant  $Z_h$ , see Eqs. (3.13). Since the graphs containing propagator  $\langle vv \rangle_0$  appear to be equal to zero, obtained answer for  $Z_h$  coincides with the corresponding answer in the model without the turbulent motion of the environment [46].

In the end of this section we have to consider the graphs corresponding to the function  $\langle h'hu \rangle_{1-ir}$ . The only difference between them and graphs  $\tilde{D}_3 - \tilde{D}_5$  for the function  $\langle h'hh \rangle_{1-ir}$  is the presence of the external field  $v$  instead of the field  $h$ . The cores of the graphs are the same. Thus,  $Z_v = Z_h$ .

## REFERENCES

- 
- [1] P. Bak, C. Tang and K. Wiesenfeld, Phys. Rev. Lett. **59**, 381 (1987).
  - [2] C. Tang, P. Bak, Phys. Rev. Lett. **60**(23), 2347 (1988).
  - [3] P. Bak, K. Sneppen, Phys. Rev. Lett. **71**(24), 4083 (1993).
  - [4] P. Bak, *How Nature Works: The Science of Self-Organized Criticality* (Copernicus, N.Y., 1996).
  - [5] H. J. Jensen, *Self-Organized Criticality: Emergent Complex behavior in Physical and Biological Systems* (Cambridge University Press, Cambridge, 1998).
  - [6] D. L. Turcotte, Rep. Prog. Phys. **62**, 1377 (1999).
  - [7] G. Pruessner, *Self-Organized Criticality: Theory, Models and Characterisation* (Cambridge University Press, 2012).
  - [8] N.W. Watkins, G. Pruessner, S.C. Chapman, et al, Space Sci. Rev. **198**, 3 (2016)
  - [9] M. A. Munoz, Rev. Mod. Phys. **90**, 031001 (2018).
  - [10] D. Markovic, C. Gros, Phys. Rep. **536**, 41 (2014).
  - [11] M. J. Aschwanden, *Self-Organized Criticality Systems* (Open Academic Press, 2013).
  - [12] D. J. Amit, *Field Theory, Renormalization Group, and Critical Phenomena* (World Scientific, Singapore, 1984) (2nd edition).
  - [13] J. Zinn-Justin *Quantum Field Theory and Critical Phenomena* (Clarendon Press, Oxford, 1989)
  - [14] A.N. Vasiliev *The Field Theoretic Renormalization Group in Critical behavior Theory and Stochastic Dynamics* (Chapman & Hall/CRC, Boca Raton, 2004)
  - [15] G. F. R. Ellis, J. Kopel, Front. Physiol. **9**, 1966 (2019).
  - [16] T. Mora, W. Bialek, J. Stat. Phys. **144**, 268 (2011).
  - [17] J. Hesse, T. Gross, Front. Syst. Neurosci. **8**, 166 (2014).
  - [18] V. Pasquale, P. Massobrio, L. L. Bologna, M. Chiappalone, S. Martinoia, Neuroscience **153**, 1354 (2008).
  - [19] J. G. Orlandi, J. Soriano, E. Alvarez-Lacalle, S. Teller, J. Casademunt, Nat. Phys. **9**, 582 (2013).
  - [20] N. M. Timme, N. J. Marshall, N. Bennett, M. Ripp, E. Lautzenhiser, J. M. Beggs, Front. Physiol. **7**, 425 (2016).
  - [21] F. Y. K. Kossio, S. Goedeke, B. van den Akker, B. Ibarz, R.-M. Memmesheimer, Phys. Rev. Lett. **121**, 058301 (2018).
  - [22] A. Levina, J. M. Herrmann, T. Geisel, Nat. Phys. **3**, 857 (2007).
  - [23] B. Tadić, M. Mitrovic Dankulov, R. Melnik, Phys. Rev. E **96**, 032307 (2017).
  - [24] B. Tadić, European Journal of Physics **40**, 024002 (2019).
  - [25] B. Tadić, V. Gligorijevic, M. Mitrovic, and M. Suvakov, Entropy **15**, 5084 (2013).
  - [26] M. Suvakov, B. Tadić, Condens. Matter Phys. **17**, 33801 (2014).
  - [27] Yu. Holovatch, O. Mrygold, M. Szell, S. Thurner, *Math Meets Myths: Quantitative Approaches to Ancient Narratives* edited by R. Kenna (Springer International Publishing, 2017).
  - [28] G. Kou, Y. Zhao, Y. Peng, Y. Shi, PLoS One **7**, e43507 (2012).
  - [29] J. M. Torres-Rojo, R. Bahena-Gonzalez, Agricultural Systems **165**, 33 (2018).
  - [30] L. Tonello, L. Giacobbi, A. Pettenon, A. Scuotto, M. Cocchi, F. Gabrielli, and G. Cappello, Complexity **2018**, 5128157 (2018).
  - [31] T. Halpin-Healy, Y.-C. Zhang, Phys. Rep. **254**, 215 (1995).

- [32] D. Forster, D. R. Nelson, M. J. Stephen, *Phys. Rev.* **16**, 732 (1977).
- [33] M. Kardar, G. Parisi, Y.-C. Zhang, *Phys. Rev. Lett.* **56**, 889 (1986).
- [34] K. J. Wiese, *Phys. Rev. E* **93**, 042117 (2016).
- [35] S. Chatterjee, A. Das, P. Pradhan, *Phys. Rev. E* **97**, 062142 (2018).
- [36] P. Le Doussal, K. J. Wiese, *Phys. Rev. Lett.* **114**, 110601 (2015).
- [37] T. Hwa, M. Kardar, *Phys. Rev. Lett.* **62**(16) 1813 (1989).
- [38] T. Hwa, M. Kardar, *Phys. Rev. A* **45**, 7002 (1992).
- [39] B. Tadić, *Phys. Rev. E* **58**, 168 (1998).
- [40] R. Pastor-Satorras, D. H. Rothman, *Phys. Rev. Lett.* **80**, 4349 (1998).
- [41] R. Pastor-Satorras, D. H. Rothman, *J. Stat. Phys.* **93**, 477 (1998).
- [42] N. V. Antonov, P. I. Kakin, *Theor. Math. Phys.* **190**(2), 193 (2017).
- [43] N. V. Antonov, P. I. Kakin, *J. Phys. A: Math. Theor.* **50**, 085002 (2017).
- [44] C. Duclut, B. Delamotte, *Phys. Rev. E* **96**, 012149 (2017).
- [45] P. I. Kakin, N. M. Lebedev, *Vestnik of Saint-Petersburg University. Series 4: Physics. Chemistry.* **4**(62)4, 398 (2017).
- [46] N.V. Antonov, P.I. Kakin, N.M. Lebedev, *J. Stat. Phys.* **178**, 392 (2020).
- [47] G. Caldarelli, A. Giacometti, A. Maritan, I. Rodriguez-Iturbe, and A. Rinaldo, *Phys. Rev. E* **55**(5), R4865(R) (1997).
- [48] A. Czirok, E. Somfai, and J. Vicsek, *Phys. Rev. Lett.* **71**, 2154 (1993).
- [49] H. Hinrichsen, *Adv. Phys.* **49** 815-958 (2000).
- [50] H. Jeong, B. Kahng, D. Kim, *Phys. Rev. Lett.* **25**, 5094 (1996).
- [51] H.-J. Kim, I.-m. Kim, J. M. Kim, *Phys. Rev. E* **58**, 1144 (1998).
- [52] O. Narayan, D. S. Fisher, *Phys. Rev. B* **48** 7030 (1993).
- [53] H. K. Janssen, *Phys. Rev. E* **55**(5) 6253 (1997).
- [54] A. G. Moreira, R. Dickman, *Phys. Rev. E* **54**, R3090 (1996).
- [55] I. Webman, D. ben Avraham, A. Cohen, S. Havlin, *Phil. Mag. B* **77**, 1401 (1998).
- [56] N. V. Antonov, N. M. Gulitskiy, M. M. Kostenko, and A. V. Malyshev, *Phys. Rev. E* **97**, 033101 (2018).
- [57] N. V. Antonov, N. M. Gulitskiy, and A. V. Malyshev, *EPJ Web of Conf.* **126**, 04019 (2016).
- [58] A. Ales, J. M. Lopez, *Phys. Rev. E* **99**, 062139 (2019).
- [59] G. Satten, D. Ronis, *Phys. Rev. Lett.* **55**, 91 (1985).
- [60] G. Satten, D. Ronis, *Phys. Rev. A* **33**, 3415 (1986).
- [61] A. Onuki, K. Yamazaki, K. Kawasaki, *Ann. Phys.* **131**, 217 (1981).
- [62] A. Onuki, K. Kawasaki *Progr. Theor. Phys.* **63**, 122 (1980).
- [63] D. Beysens, M. Gbadamassi, L. Boyer, *Phys. Rev. Lett* **43**, 1253 (1979).
- [64] R. Ruiz, D.R. Nelson, *Phys. Rev. A* **23**, 3224 (1981).
- [65] A. Aronowitz, D. R. Nelson, *Phys. Rev. A* **29**, 2012 (1984).
- [66] N. V. Antonov, M. Hnatich, J. Honkonen, *J. Phys. A: Math. Gen.* **39**, 7867 (2006).
- [67] N.V. Antonov, A.A. Ignatieva, *J. Phys. A: Math. Gen.* **39**, 13593 (2006).
- [68] N. V. Antonov, V. I. Iglovikov, A. S. Kapustin, *J. Phys. A: Math. Theor.* **42**, 135001 (2008).
- [69] N.V. Antonov, A.S. Kapustin, A.V. Malyshev, *Theor. Math. Phys.* **169**, 1470 (2011).
- [70] N.V. Antonov, P.I. Kakin, *EPJ Web of Conferences* **108**, 02009 (2016).
- [71] M. Avellaneda, A. Majda, *Commun. Math. Phys.* **131**, 381 (1990).
- [72] M. Avellaneda, A. Majda, *Commun. Math. Phys.* **146**, 139 (1992).
- [73] G. Falkovich, K. Gawędzki and M. Vergassola, *Rev. Mod. Phys.* **73**, 913 (2001).
- [74] A. Majda, *SIAM Rev.* **33**, 349 (1991).
- [75] A. Majda, *J. Stat. Phys.* **73**, 515 (1993).
- [76] A. Majda, *J. Stat. Phys.* **75**, 1153 (1994).
- [77] M. Avellaneda, A. Majda, *Phil. Trans. Roy. Soc. London A* **346**, 205 (1994).
- [78] M. Avellaneda, A. Majda, *Phys. Fluids A* **4**, 41 (1992).
- [79] M. Avellaneda, A. Majda, *Phys. Rev. Lett.* **68**, 3028 (1992).
- [80] D. Hornthrop and A. Majda, *J. Math. Sci. Univ. Tokyo* **1**, 23 (1994).
- [81] Q. Zhang, J. Glimm, *Commun. Math. Phys.* **146**, 217 (1992).
- [82] T. C. Wallstrom, *Proc. Natl. Acad. Sci. USA* **92**, 11005 (1995).
- [83] N. V. Antonov, A. A. Ignatieva, A. V. Malyshev, *Physics of Particles and Nuclei* **41**, 998 (2010).
- [84] N.V. Antonov, A.V. Malyshev, *Theor. Math. Phys.* **167**, 444 (2011).
- [85] N.V. Antonov, A.V. Malyshev, *J. Phys. A: Math. Theor.* **45** 255004 (2012).
- [86] N.V. Antonov, A.V. Malyshev, *J. Stat. Phys.* **146**, 33 (2012).
- [87] N. V. Antonov and N. M. Gulitskiy, *Phys. Rev. E* **91**, 013002 (2015).
- [88] N. V. Antonov and N. M. Gulitskiy, *Phys. Rev. E* **92**, 043018 (2015).
- [89] N. V. Antonov, N. M. Gulitskiy, *AIP Conf. Proc.* **1701**, 100006 (2016).
- [90] N. V. Antonov, N. M. Gulitskiy, *EPJ Web of Conf.* **108**, 02008 (2016).
- [91] N. V. Antonov, *Phys. Rev. E* **60**, 6691 (1999).
- [92] N. V. Antonov, *Physica D* **144**, 370 (2000).
- [93] L. Ts. Adzhemyan, N. V. Antonov, J. Honkonen, *Phys. Rev. E* **66**, 036313 (2002).
- [94] N. V. Antonov, M. Hnatich, J. Honkonen, M. Jurcisin, *Phys. Rev. E* **68**, 046306 (2003).
- [95] N.G. Van Kampen, *Stochastic Processes in Physics and Chemistry* (North Holland, 2007) (3rd edition).

- [96] C. Gardiner, *Stochastic Methods: A Handbook for the Natural and Social Sciences*, (Springer, 2009) (4th edition).
- [97] P.C. Martin, E.D. Siggia, and H.A. Rose, *Phys. Rev. A* **8**, 423 (1973).
- [98] C. De Dominicis, *J. Phys. (Paris)* **C1**, 247 (1976).
- [99] H.K. Janssen, *Z. Phys. B* **23**, 377 (1976).
- [100] M. Holzer, E. D. Siggia, *Phys. Fluids* **6**, 1820 (1994).
- [101] M. Hnatic, J. Honkonen, and T. Lucivjansky, *Symmetry* **11**, 1193 (2019).
- [102] C. De Dominicis and P.C. Martin, *Phys. Rev. A* **19**, 419 (1979).
- [103] L.Ts. Adzhemyan, N.V. Antonov, and A.N. Vasil'ev, *Quantum field renormalization group in the theory of fully developed turbulence*. *Physics-Uspekhi* **39**, 1193 (1996) [Translated from the Russian: *Uspekhi Fiz. Nauk*, **166**(12) 1257 (1996)].
- [104] L.Ts. Adzhemyan, N.V. Antonov, and A.N. Vasil'ev, *The Field Theoretic Renormalization Group in Fully Developed Turbulence* (Gordon and Breach, London, 1999).